Journal of Power Sources 196 (2011) 4886–4904

Contents lists available at ScienceDirect

Journal of Power Sources

journal homepage: www.elsevier.com/locate/jpowsour

Review

Electrospinning materials for energy-related applications and devices

Zexuan Dong[a], Scott J. Kennedy[b], Yiquan Wu[a,*]

[a] Materials Science Program, Department of Mechanical Engineering, University of Rochester, Rochester, NY 14627, USA
[b] Department of Mechanical Engineering and Material Science, Duke University, Durham, NC 27708, USA

ARTICLE INFO

Article history:
Received 29 November 2010
Accepted 24 January 2011
Available online 24 February 2011

Keywords:
Electrospinning
Fuel cells
Dye-sensitized solar cells
Lithium-ion batteries
Supercapacitors
Thermoelectric

ABSTRACT

The tasks of harvesting, transmitting, and storing the energy required to meet global demands are some of the most pressing needs we will face in the near future. Scientists are seeking new technologies to generate renewable and clean energy resources. Nanofiberous materials with high surface areas and porosities have attracted significant attention in recent years and are considered to be promising candidates to address these critical issues. Nanofibers can be produced by many techniques. Of these, electrospinning is a particularly low cost and versatile method. This paper highlights research into the use of electrospinning to create materials suited for four major energy-related applications: (1) fuel cells, (2) dye-sensitized solar cells, (3) Li-ion batteries, and (4) supercapacitors. In addition, electrospun nanofibers used in other areas, such as thermoelectrical and piezoelectric materials, are also discussed. Specific attention is given to the material properties that have been achieved through electrospinning and what limitations of existing processes offer opportunities for future research.

Contents

* Corresponding author. Tel.: +1 585 275 4844; fax: +1 585 256 2509.
E-mail address: wuyiquan@me.rochester.edu (Y. Wu).

0378-7753/$ – see front matter © 2011 Elsevier B.V. All rights reserved.
doi:10.1016/j.jpowsour.2011.01.090

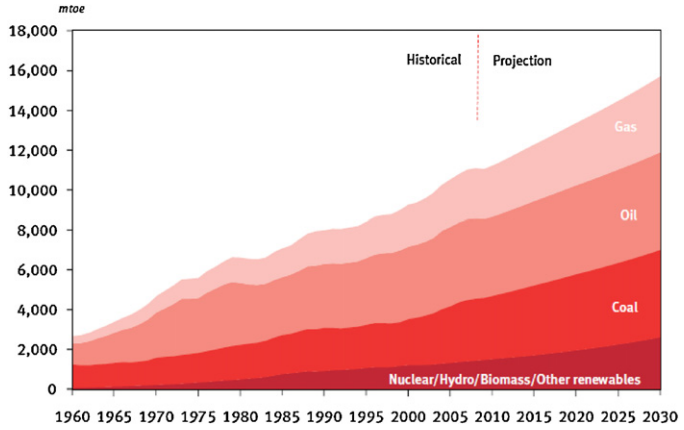

Fig. 1. World supply of primary energy by fuel type (from Ref. [1]).

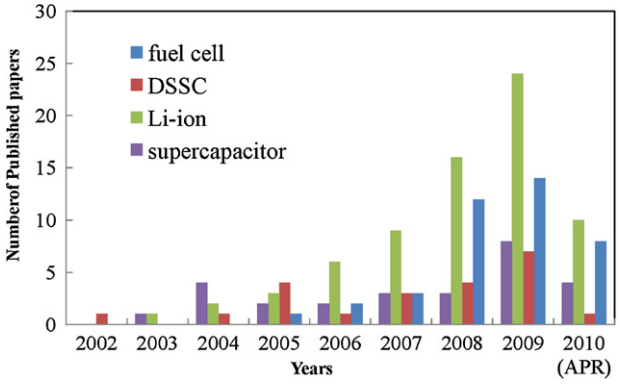

Fig. 2. Research articles published on the use of electrospun nanofibers in energy conversion devices and materials. (Search made through ISI Web of Science database.)

1. Introduction

In both scientific and popular literature, issues stemming from globalization and global population projections have prompted dramatic predictions and speculation regarding changes to our ways and quality of life. Energy issues are central to discussions regarding the long-term sustainability of current environmental and economic behaviors and our need to produce and transport sufficient food and water to larger and increasingly urban global populations. Energy is a vital factor in all areas of modern life including how we address needs as basic as food and water. The use of petrochemical fertilizers and the mechanization of farming have revolutionized crop production while the production of biofuels further intertwines the relationship between energy and food production. Energy is critical to many ideas of future seawater desalinization in regions where potable water is becoming increasingly scarce. Although the use of new energy resources are projected to grow at fast rates, fossil fuels, particularly oil and coal, are expected to play a leading role through 2030, contributing more than half of the global energy supply [1] (Fig. 1 and Table 1).

The growth of oil production and its steadily dropping prices from 1920 through 1973 has played an important role in promoting global economic growth. However, the population has nearly quadrupled and energy demand has increased exponentially in the 20th century. According to the US Energy Information Administration, in 2006, global energy consumption was approximately 500 exajoules, of which about 86% came from fossil fuels, such as oil, coal and natural gas. This number is expected to increase to 580 exajoules by 2015 and 720 exajoules by 2030; a 44% increase in only 24 years [2]. Of course, the reserve of fossil fuels and our ability to harvest it is not infinite. Even if it were infinite, it is important to consider the impact of increasing the usage of fossil fuels on our environment. The use of fossil fuels contributes to air and water pollution and to higher carbon dioxide concentrations, which have been estimated to contribute 9–26% to the global greenhouse effect [3].

While the global fossil fuel supply will not be exhausted anytime in the near future, it is critical that the development of advanced energy technologies outpace the onset of potential energy shortages. In addition to transitioning from fossil fuel sources to new energy resources such as wind, solar and tidal power, technology and devices must be developed for clean energy-conversion, storage and conservation. There are promising clean alternative energy devices such as fuel cells, solar cells, and lithium-ion batteries. Although these developing energy technologies represent important steps towards meeting our energy demands, new breakthroughs are needed to improve their performance in terms of durability, harvest efficiency, power density, conversion efficiency and cost. In order to overcome these challenges, researchers have worked to create new nanosized functional materials. Nanomaterials have very high surface area to volume ratios, which result in special properties in comparison to bulk materials. An excellent example of this is the absorption of solar radiation in photovoltaic cells, which is much higher in structures composed of nanoparticles than it is in continuous sheets of thin film material. In this case, the smaller the particles are, the greater the solar energy absorption. There are many kinds of nanoscale materials including nanoparticles, nanopowders, nanorods, nanotubes, and nanowires. Nanoparticles (zero-dimensional) have been intensively studied for a long time, while one-dimensional (1D) nanomaterials have attracted attention from researchers and scientists recently. Nanomaterials and films composed of 1D materials can be used in various applications where high surface area and porosity are desirable. 1D nanomaterials can be prepared by many methods such as template-directed methods [4–6], vapor-phase methods [7], interface synthesis techniques [8], solvothermal synthesis [9], solution-phase growth controlled by capping reagents [10], nanolithography [11,12] and self-assembly [13]. However, each of these methods has limitations, such as material restrictions, high cost, and high process complexity. Recently, electrospinning, a simple, inexpensive technique, has attracted significant attention in the preparation of nanomaterials. It has been used to make nanofibers, nanotubes, nanobelts and porous membranes. These electrospun nanomaterials have unique properties applicable to a wide range of fields, including the fabrication of nanomaterials for use in energy conversion devices. Fig. 2 illustrates the recent growth in the number of papers published on the application of electrospun materials in energy conversion devices. This review surveys the materials resulting from electrospinning techniques that hold promise for energy conversion applications.

2. Principle and applications of electrospinning

The field of electrospinning traces its roots back to an initial patent on the electrical dispersion of fluids from 1902 [14]. The fabrication of textile yarns from electrically dispersed fluids was patented by Formhals in 1934 [15]. However, this technique did not receive much attention until the 1990s, when several research groups (notably that of Reneker) [16,17] found that it could be used to generate nanofibers from many organic polymers. Since then, the term “electrospinning” has been popularized and the number of publications about electrospinning has increased dramatically each year. Today, electrospinning is an established technique for generating nanofibers [16,18–20].

Table 1
World supply of primary energy by reference case (from Ref. [1]).

	Levels (mtoe)				Growth (%p.a.)	Fuels shares (%)			
	2007	2010	2020	2030	2007–2030	2007	2010	2020	2030
Oil	4,045	3,967	4,457	4,902	0.8	36.4	35.1	33.1	31.0
Coal	3,129	3,225	3,871	4,438	1.5	28.2	28.5	28.8	28.1
Gas	2,479	2,551	3,124	3,808	1.9	22.3	22.6	23.2	24.1
Nuclear	736	759	873	1,065	1.6	6.6	6.7	6.5	6.7
Hydro	268	289	366	448	2.3	2.4	2.6	2.7	2.8
Biomass	394	446	618	840	3.4	3.5	3.9	4.6	5.3
Other renewables	59	73	151	303	7.4	0.5	0.6	1.1	1.9
Total	11,109	11,310	13,461	15,804	1.5	100.0	100.0	100.0	100.0

A typical electrospinning apparatus consists of a syringe, a grounded collector and a high voltage power supply. A schematic of an electrospinning set up is shown in Fig. 3. In a typical fiber-spinning process, a syringe is filled with a melt or blend polymer solution and a high voltage (typically kV) is applied between the syringe nozzle and a collector. Electrospinning is fundamentally different from air or other mechanically driven spinning techniques in that the extrusion force is generated by the interaction between the charged polymer fluid and an external applied electric field. During electrospinning, a conical fluid structure called the Taylor cone [21] is formed at the tip of the syringe. At a critical voltage, the repulsive force of the charged polymer overcomes the surface tension of the solution and a charged jet erupts from the tip of the Taylor cone. If the applied voltage is not high enough, the jet will break up into droplets, a phenomenon called Rayleigh instability. If the voltage is sufficiently high, a stable jet will form near the tip of the Taylor cone. Beyond the stable region, the jet is subject to bending instability [22] that results in the polymer being deposited on the grounded collector via a whipping motion. As the charged jet accelerates towards regions of lower potential, the solvent evaporates, and the resulting increase in the electrostatic repulsion of the charged polymer causes the fibers to elongate. The strength of the polymer chains prevents the jet from breaking up resulting in the formation of fibers.

Almost any soluble polymer can be electrospun if its molecular weight is high enough. However, the creation of fine nanofibers requires the careful consideration of many operating parameters (such as polymer molecular weight, applied voltage, solution feed rate and spinning distance), environmental parameters (such as temperature, humidity and air velocity in the chamber) and solution properties (such as conductivity, viscosity and surface tension). By selecting different polymer blends and tuning these electrospinning process parameters, a wide range of nanofibers made of natural polymers, polymer blends, ceramic precursors and metal or metal oxides have been spun into an assortment of different fiber morphologies, such as beaded [23,24], ribbon [24,25], porous [26,27], core–shell [27] and aligned [28] fibers (Fig. 4). Because electrospun membranes have nanofibrous structure similar to human tissues and organs [18], they are well suited for use in many biomedical applications. Statistics show that about 40–60% [18,29] of electrospinning publications focus on applications such as tissue engineering [30–32], medical prostheses [33], drug delivery [34–36], and wound healing [35,37,38]. In addition to biomedical applications, they have also been used in other areas such as sensors [39–41], filters and separation membranes [42,43], templates for nanotube materials [44], protective layer [45], composite materials [46,47] and energy applications [29,48]. The applications of electrospinning relating to energy and environmental areas have already been discussed in a thorough review [29], however, in this paper, we focus specifically on the subject of electrospun fiberous materials in energy conversion devices (mainly fuel cells, solar cells and lithium-ion cells). Tables 2 and 3 provide a summary of the content in this paper.

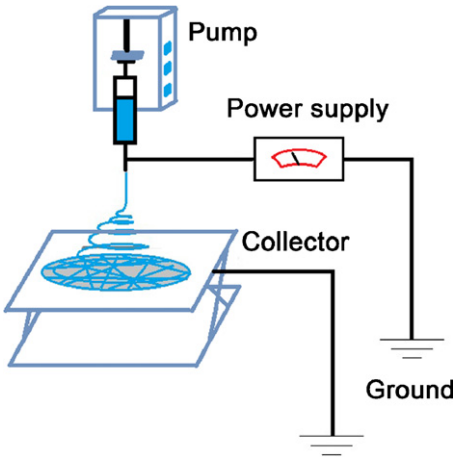

Fig. 3. Schematic diagram of an electrospinning apparatus.

3. Applications

3.1. Fuel cells

A fuel cell is an energy conversion device where electrochemical oxidation of hydrogen or hydrogen-rich fuel is converted into electrical energy. Fuel cells are different from conventional electrochemical cell batteries; rather than rely on static stores of chemicals that must be periodically recharged or replaced, fuel cells require a flow of chemicals (e.g., hydrogen and oxygen) that react in the presence of catalysts. Electricity is generated through the reaction, and conducted to an external circuit. If the necessary reactants are maintained, fuel cells can theoretically operate continuously.

There are many types of fuel cells, such as: proton exchange membrane (PEM) fuel cells, alkaline fuel cells, phosphoric acid fuel cells, molten carbonate fuel cells, and solid oxide fuel cells. PEM fuel cells have attracted the most research attention, because of their high-power density and low operating temperature. In this review, we will primarily (though not exclusively) discuss the applications of electrospinning in PEM fuel cells. Typically, a PEM fuel cell is composed of a five-layer membrane electrode assembly (MEA, including a proton exchange membrane, two catalyst layers, and two gas diffusion layers), two graphite plates and other assisting components, such as gasketing. Of those, the catalyst layers, their supporting substrate and the proton exchange membrane are the most critical components. A schematic of a PEM fuel cell is shown in Fig. 5.

3.1.1. Catalyst

The catalyst material is the key component in a PEM fuel cell. It facilitates the reaction of oxygen and hydrogen. Usually, com-

Table 2
Applications of electrospun materials in fuel cells, solar cells and lithium-ion cells. Micro-structure descriptions include diameter, *D*, specific surface area, SSA and conductivity, *C*.

Applications	Materials	Micro-structure	Advantages	Reference
Fuel cells: catalyst (electrodes)	PtRh, PtRu	*D* 50 nm	High mass activity	[49]
	Pt	*D* 25–35 nm	High power density	[50]
	Pt	*D* 5–20 nm	Free-standing catalyst	[51]
	Pt	*D* 20–40 nm	Efficient charge and mass transport, high ORR activity	[52]
Fuel cells: supporting materials	TiO_2	*D* 150–400 nm	Improved electrochemical activity and durability	[62]
	CNF	*D* (Average) 250nm; SSA 307 $m^2\ g^{-1}$	High Pt utilization, high catalytic activity	[65]
	CNF/Ni	*D* 100–300 nm; SSA 480–682 $m^2\ g^{-1}$	Improved physical and thermo-chemical properties	[66]
	CNF		Improved Pt loading	[67]
	CNF	*D* 130–170 nm; C 55 S cm^{-1}	High electrocatalytic activity and stability	[68]
	CNF	*D* 100–300 nm	High electrical and thermal conductivities, and good electrochemical stability	[69]
	CNF	*D* (Average) 118 nm	Higher catalytic activities than that obtained on conventional carbon supports	[71]
	PAN	*D* 740 nm	High porosity and high surface areas	[70]
	PA6	*D* (Average) 152 nm	Excellent mechanical properties, good conductivity, and high porosity	[72]
	PS	*D* 3–4 μm	Robust porous media, and pore size can be controlled	[73]
Fuel cells: polymer membrane	Nafion/PAA	*D* 100–600 nm		[142]
	Nafion/PEO,PVA, PVP	*D* 500 nm–2 μm	Increased the PEMFC current density	[75]
	Nafion/PVdF		Blocks the methanol crossover	[76]
	PVdF/PWA		Fewer beads	[77]
	NTDA-BDSA-r-APPF	Aligned, *D* 199 ± 37 nm	High proton conductivity, low gas permeability	[78]
DSSCs: photoelectrode	TiO_2	*D* 50 nm–2 μm	High specific surface area, controllable pore sizes	[94]
	TiO_2	*D* (Average) 150 nm	High effective electron diffusion coefficients	[81]
	TiO_2		Enhanced penetration of electrolyte, increase in sensitizer adsorption	[80,95–98]
	TiO_2	Aligned, *D* (Average) 45 nm	Low electrical resistance, high cell performance	[99]
	TiO_2	Ground, *D* 150 ± 60 nm	Better adhesion	[100]
	TiO_2	Fiber/particle, *D* ~250 nm	High surface area	[88]
	TiO_2	*D* 150–700 nm	High surface area	[102]
	TiO_2	*D* ~90 nm		[103]
	TiO_2	SSA 123 $m^2\ g^{-1}$	Higher sensitizer surface, longer recombination lifetime	[104]
	TiO_2/MWCNT	*D* 65 ± 35 nm	Longer recombination lifetime, high surface area, enhanced surface activities	[106]
	ZnO	*D* 200–500 nm		[108]
	ZnO	SSA 30.0 $m^2\ g^{-1}$	Direct conduction pathway	[109]
	PVP/$RuL_2(NCS)_2$,TiO_2	*D* 300–500 nm	Combines the advantages of 1D nanostructures, organic and inorganic materials	[114]
DSSCs: electrolyte	PVdF-HFP	*D* 600 nm	No leakage, good durability	[82]
	PvdF-HFP	*D* (Average) 800–1000 nm	Low cost	[116,117]
Li-ion batteries: cathode materials	$LiCoO_2$	*D* 500 nm–2 μm	More Li^+ cations insertion and faster solid-state diffusion	[124]
	$LiCoO_2$	*D* 100–150 nm	High surface area	[125]
	$LiCoO_2$	*D* 60–80 nm	Higher intercalation voltage, higher energy density	[126]
	$LiCoO_2$/MgO	Core–shell *D* 1–2 μm	Core–shell, enhances the structural stability	[129]
	$LiNi_{1/3}Co_{1/3}Mn_{1/3-x}Al_xO_2$	*D* 100 nm	High specific surface area	[132]
	$LiFePO_4$/C	Core–shell structure	High current density	[135]
Li-ion batteries: anode materials	C/Si		High accessible surface area, high reversible capacity, and relatively good cycling performance	[138]

Table 2 (*Continued*)

Applications	Materials	Micro-structure	Advantages	Reference
	C/Si		High interfacial surface area, short lithium ion diffusion distance	[139]
	C/Si		Controllable size and high surface areas	[140]
	C/Fe_3O_4	*D* ~350 nm	Digests the volume change during the conversion reaction	[142]
	C/MnO_x	*D* 120–200 nm	Highly developed internal surface area, good mechanical stability, and high electrical conductivity	[143,144]
	C/Ni		High reversible capacity, low irreversible capacity, slow fading after prolonged cycling, excellent rate capacity	[146]
	C/Sn	Multichannel tubular, *D* 2 μm	Porous carbon shell maintains the stability of the structural arrangement	[148]
	C/Sn	Hollow CNFs, *D* 150 nm	High electrode–electrolyte contact	[149]
	C/Sn	Tens to hundreds of nanometers	Binder free, enhances the conductivity of the electrode	[150]
	C/Cu		Enhanced surface-to-volume ratio, numerous active sites, facile electronic/ionic transfer, high conductivity	[147]
	C/Co	*D* 100–300 nm	Reduced Li-ion diffusion distance	[151]
	C/Mn_3O_4	*D* 200–300 nm	Large surface-area-to-volume	[156]
	Porous C	*D* 200–300 nm, SSA 235 $m^2\ g^{-1}$	Ultrahigh surface area and porosity, fast electron transfer rate	[157–159]
	TiO_2	*D* (Average) 100 nm	Smooth intercalation of lithium ions in the nanofiber based TiO_2	[162]
	Co_3O_4	*D* 600 nm–1 μm, 200	Increased specific strength	[164,165]
	NiO/SWCNT	*D* 40–50 nm	Pulverization prevented, improved conductivity	[155]
Li-ion batteries: electrolyte	PVdF	*D* (Average) 250 nm	High porosity, high surface area, interconnected pores, sufficient mechanical strength	[167]
	PVdF	*D* 514–884 nm	80% porosity, high ionic conductivity	[168]
	PVdF-g-tBA		Considerable ionic conductivity	[169]
	P(VdF-HFP)	*D* (Average) 0.5 μm, 1.3 μm	High specific surface area, high porosity, and unique tortuosity of the pore structure	[170]
	P(VdF-HFP)	*D* (Average) ~2 μm	High surface area, fully interconnected pore structure	[171]
	P(VdF-HFP)/PMMA	*D* 200–350 nm		[172]
	P(VdF-HFP)/SiO_2	*D* (Average) 3–5 μm	High surface area fibers, interconnected pore structures	[177]
	P(VdF-HFP)/SiO_2	*D* 1–2 μm	High specific surface area, large porosity	[178]
	PVdF	*D* 540–1280 nm	High surface area fibers, interconnected pore structures	[179]
	PVdF/PAN	*D* 250–400 nm	Induced phase mixing between PVdF and PAN	[173]
	PAN	*D* 350 nm, porosity ~70%	Close thickness and pore size	[180]
	PAN	*D* 250, 380 nm, pore size 0.17, 0.28, 0.38 μm	Small pore size, small volume, high porosity and high air permeability	[181]
	PVdF/OC/TPGDA	*D* 100–400 nm	Microporous structure	[174]
	PPy/SEBS	*D* 200–500 nm	High specific surface area, large aspect ratio, contact efficiency, and dimensional stability	[182]
Super capacitors: electrode	CNF	*D* ~250 nm	High specific surface area	[187,188]
	CNF	*D* ~100 nm, SSA 310–550 $m^2\ g^{-1}$	High accessible surface area and relatively high electrical conductivities	[189]
	CNF	*D* 1–2 μm, SSA 600–1450 $m^2\ g^{-1}$	High porosities and high surface-to-area ratios	[191]
	CNF	*D* 250–300 nm, SSA 460–1160 $m^2\ g^{-1}$	High specific surface area resulting from shallow pore size	[190]
	CNF/Ru	*D* 100–350 nm	Expansion of the pore diameter	[192]
	CNF/Ni		Improved physical and thermo-chemical properties	[66]
	CNF/Ni	*D* 100–300 nm; SSA 480–682 $m^2\ g^{-1}$	High surface area-to-volume ratio	[193]
	NiO/P(VdF-HFP)/C	*D* ~150 nm	High specific surface area	[194]
	CNF/MWCNT	*D* 100–400 nm	High surface area	[195]
	PPy/ACNF/CNT	*D* 50–200 nm	High surface area, average pore diameter and high electrical conductivity	[196]
	CNF/MWCNT	*D* (Average) 230 nm; SSA 1170 $m^2\ g^{-1}$	Freestanding, high porosity and specific surface area	[197]
	$SrRuO_3$–RuO_2	*D* 20–50 nm	Simple, cost-effective	[199]

Table 2 (*Continued*)

Applications	Materials	Micro-structure	Advantages	Reference
Piezoelectric materials	Perovskite lead zirconate titanate (PZT)	*D* 200–300 nm	Fibrous structure offers both damping and reinforcement in composite fabrication.	[201]
	PZT	*D* 52–150 nm, aligned	Increased anisotropy, excellent flexibility and improved strength	[202]
	PZT	*D* 150–1250 nm	Excellent flexibility and strength	[203]
	$Bi_{3.15}Nd_{0.85}Ti_3O_{12}$	*D* 30–200 nm	Directly synthesize ferroelectric nanofibers on substrates	[204]
	V-ZnO	50–300 nm	Excellent physical and chemical properties in nanoscale device applications	[205,206]
Thermoelectric materials	$NaCo_2O_4$	*D* 20–200 nm	Potential applications in thermoelectric nanodevices	[207]
	$Ca_3Co_4O_9$	*D* ~200 nm	Much smaller grain size, controlled grain orientation	[211]

mercial PEM fuel cells use Pt nanoparticles as catalyst, but these catalysts may suffer from poor durability. Electrospinning has been used to develop new catalysts with high activity, high poisoning resistance and good durability. Kim et al. electrospun PtRu [49], PtRh [49,50] and Pt nanowires [50]. These nanowire catalysts had average diameters of 30–40 nm and showed better performance than conventional carbon-supported Pt or Pt black. The enhanced electrical properties and pertinent interface formation with nanowire catalysts are believed to contribute to the improved performance in fuel cell systems. In another paper, ultrathin, uniform Pt nanowires were electrospun from a PVP/H_2PtCl_6 system in an investigation that highlighted the mechanism of bead formation [51]. Fig. 6 illustrates TEM images of electrospun PtRh and Pt nanowires. Since 1-dimentional materials have smaller specific surface areas than particles, catalyst particles deposited on catalyst nanowires may be a good method for combining the advantages of both nanowires and nanoparticles. Kim et al. proposed a method to make Pt nanowire composited with Pt/C by mixing electrospun Pt nanowires and commercial Pt/C [52]. The Pt nanowires provided more efficient charge and mass transport while the Pt/C nanoparticles offered high surface area yielding a catalyst system that exhibited improved ORR activity.

3.1.2. Catalyst supporting materials

PEM fuel cell reactions require a catalyst. One significant barrier to using PEM fuel cells in practice is the high cost of noble metal catalysts, like platinum. In order to reduce the cost, much of the current research on PEM fuel cells focuses on obtaining high catalytic activity and catalyst utilization. To improve the catalyst activity, catalyst particles must be uniformly dispersed on porous support materials. Currently, most Pt nanoparticles are prepared on various carbon supports, such as Vulcan XC-72R [53], multiwall carbon nanotubes (MWCNT) [54–56], graphite nanofibers [57], activated carbon [58–60], carbon black and graphite [58]. However, carbon support materials can suffer from degradation in the harsh operating conditions of PEM fuel cells. For better stability, the use of

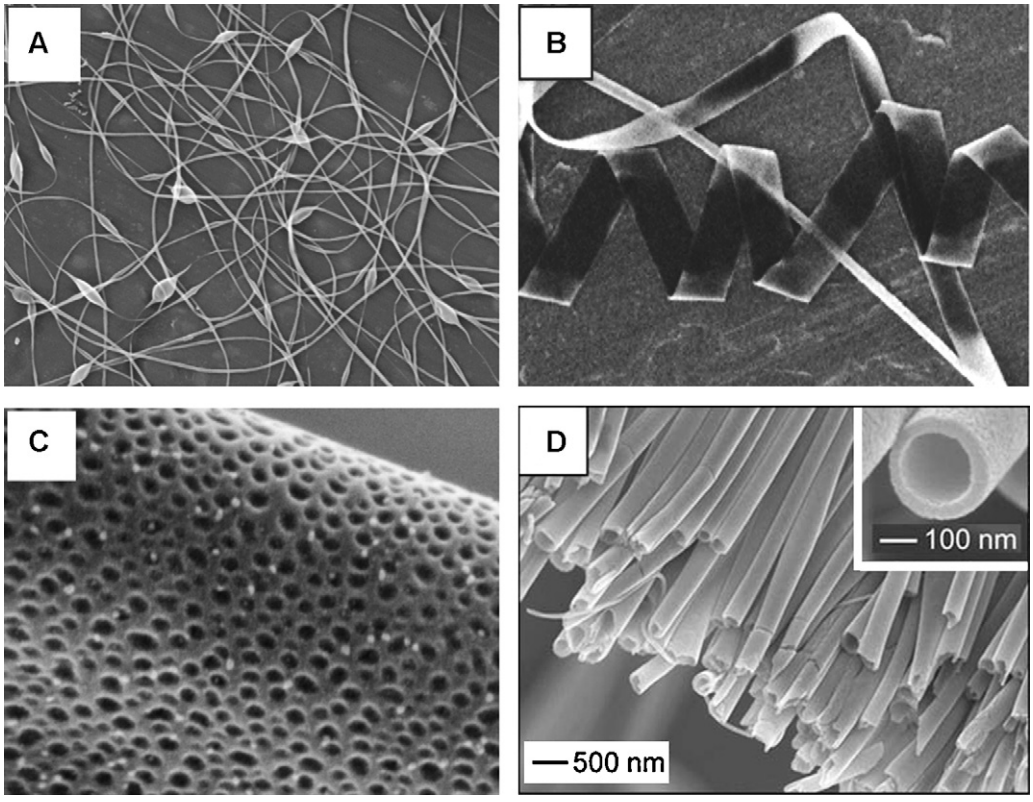

Fig. 4. Different electrospun fiber morphologies: (A) beaded (from Ref. [23]), (B) ribbon (from Ref. [24]), (C) porous fibers (from Ref. [26]) and (D) core–shell (from Ref. [27]).

Table 3
Electrospinning materials and operation parameters.

Materials	Precursors	Electrospinning parameters	Applications	References
CNF	PAN	13.7 kV, 12 cm	Pt catalyst support	[65,68]
CNF	Poly(amic acid)		Pt catalyst support	[67]
CNF	PAN	15 kV	Pt catalyst support	[69]
CNF	PAN	100 kV m^{-1}	Pt/Au catalyst support	[71]
CNF	PAN, PLLA	17 kV, 15 cm, 0.5 mL h^{-1}	Anode for Li-ion battery	[157]
CNF	PAN, $ZnCl_2$	14 kV, 15 cm, 0.5 mL h^{-1}	Anode for Li-ion battery	[158]
CNF	PAN, SiO_2	21 kV, 15 cm, 0.8 mL h^{-1}	Anode for Li-ion battery	[159]
CNF	PBI	12–15 kV	Electrode for supercapacitor	[187,188]
CNF	PAA	15 kV	Electrode for supercapacitor	[191]
CNF	PAN	20 kV	Electrode for supercapacitor	[190]
CNF/Si	PAN, PLLA, Si	21 kV, 15 cm, 0.75 mL h^{-1}	Anode for Li-ion battery	[138]
CNF/Si	PAN, Si	17 kV, 15 cm, 0.75 mL h^{-1}	Anode for Li-ion battery	[139]
CNF/Si	PVA, Si	20 kV, 11 cm, 1 mL h^{-1}	Anode for Li-ion battery	[140]
CNF/Fe_3O_4	PAN, ferric acetylacetonate	12–14 kV, 12 cm, 4 μL min^{-1}	Anode for Li-ion battery	[142]
CNF/MnO_x	PAN, $Mn(CH_3COO)_2$	21 kV, 14 kV, 15 cm, 0.75 mL h^{-1}	Anode for Li-ion battery	[143,144]
CNF/Sn	PMMA, PAN, tin octoate	15 kV, 16 μL min^{-1}	Anode for Li-ion battery	[148]
CNF/Sn	PAN, tributyltin, mineral oil	20 kV, 15 cm, 15 (outer) and 5 (inner) μL min^{-1}	Anode for Li-ion battery	[149]
CNF/Sn	PVA, $SnCl_2$ H_2O	25 kV, 15 cm, 1 mL h^{-1}	Anode for Li-ion battery	[150]
CNF/Cu	PAN, $Cu(CH_3COO)_2$	10.5 kV, 15 cm, 0.5 mL h^{-1}	Anode for Li-ion battery	[147]
CNF/Ni	$[Ni(OAc)_2]\cdot 4H_2O$, PAN	12.5 kV, 15 cm, 0.5 mL h^{-1}	Anode for Li-ion battery	[146]
CNF/Ni	PAN, nickel nitrate	25 kV, 20 cm	Electrodes, catalyst support	[66]
CNF/Ni	Nickel acetate, PAN, nickel acetate	35 kV, 20 cm, 0.5 mL h^{-1}	Electrode for supercapacitor	[193]
CNF/Co	PAN, $Co(CH_3COO)_2\cdot 4H_2O$	10–11 kV, 12 cm, 2.5 μL min^{-1}	Anode for Li-ion battery	[151]
CNF/ZnCl	PAN, zinc chloride	25 kV, 20 cm	Electrode for supercapacitor	[189]
CNF/Ru	PAN, ruthenium(III) acetylacetonate	20 kV, 18 cm, 1 mL h^{-1}	Electrode for supercapacitor	[192]
PPy/ACNF/CNT	PPy, PAN, CNT	20 kV, 15 cm, 1 mL h^{-1}	Electrode for supercapacitor	[196]
CNF/MWCNT	PAN, MWCNT	12 kV, 15 cm	Electrode for supercapacitor	[195]
CNF/MWCNT	PAN, MWCNT	30 kV, 30 cm	Electrode for supercapacitor	[197]
PAN/Au	PAN, $HAuCl_4\cdot 3H_2O$	7.5 kV, 12 cm, 1.0 mL h^{-1}	Pt catalyst support	[70]
PAN	PAN	14 kV, 8 cm, 1.2 mL h^{-1}	Polymer electrolyte membrane	[180,181]
PA6	Polyamide 6	18 kV, 10 cm, 0.3 mL h^{-1}	Pd catalyst support	[72]
PS	Styrene	10 kV, 10 cm, 0.1–15 mL h^{-1}	Pt catalyst support	[73]
PtRh	$H_2PtCl_6\cdot 6H_2O$, $RhCl_3\cdot xH_2O$, PVP	6 kV, 6 cm, 0.05 mL h^{-1}	Catalyst for DMFC	[49,50]
PtRu	$H_2PtCl_6\cdot 6H_2O$, $RuCl_3\cdot xH_2O$, PVP	6 kV, 6 cm, 0.05 mL h^{-1}	Catalyst for DMFC	[49]
Pt	$H_2PtCl_6\cdot 6H_2O$, PVP	6 kV, 6 cm, 0.05 mL h^{-1}	Catalyst for fuel cell	[50]
Pt	$H_2PtCl_6\cdot 6H_2O$, PVP	5 kV, 6 cm, 0.1 mL h^{-1}	Catalyst for fuel cell	[51]
Pt	$H_2PtCl_6\cdot H_2O$, PVP	6 kV, 6 cm, 0.05 mL h^{-1}	Catalyst for fuel cell	[52]
Mn_3O_4	Manganese(II) acetate tetrahydrate, PMMA, DMF	20 kV, 25 cm	Anode for Li-ion battery	[156]
Nafion/PAA	Nafion, poly(acrylic acid)	10–25 kV, 10–25 cm, 0.5–5 mL h^{-1}	Polymer electrolyte membrane	[74]
Nafion/PEO, Nafion/PVA, Nafion/PVP	Nafion, PEO, PVA, PVP	10.4 kV, 104 mm, 1 mL h^{-1} 20 kV, 105 mm, 0.3 mL h^{-1} 10–15 kV, 100 mm, 0.5–2 mL h^{-1}	Polymer electrolyte membrane	[75]
Nafion/PVdF	Nafion, PVdF		Polymer electrolyte membrane	[76]
PVdF PVdF/PWA	PVdF, PWA	15 kV, 15 cm, 1 mL h^{-1}	Polymer electrolyte membrane	[77]
NTDA-BDSA-r-APPF	NTDA-BDSA-r-APPF	24 kV, 10 cm, 0.12 mL h^{-1}	Polymer electrolyte membrane	[78]
PVdF-HFP	PVdF-HFP	12 kV, 12 cm	Polymer electrolyte membrane	[82]
PVdF-HFP	PVdF-HFP	8–14 kV, 13–21 cm, 2 mL h^{-1}	Polymer electrolyte membrane	[116,117]
P(VdF-HFP)	P(VdF-HFP)		Polymer electrolyte membrane	[170]
P(VdF-HFP)	P(VdF-HFP), SiO_2	18 kV	Polymer electrolyte membrane	[177]
P(VdF-HFP)/PMMA	P(VdF-HFP), PMMA	30 kV, 15 cm	Polymer electrolyte membrane	[172]
P(VdF-HFP)/SiO_2	P(VdF-HFP), tetraethoxy silane	20 kV, 16 cm, 0.1 mL min^{-1}	Polymer electrolyte membrane	[178]
P(VdF-HFP)	P(VdF-HFP)	18 kV	Polymer electrolyte membrane	[171]
PVdF	PVdF	8–15 kV, 0.1 mL min^{-1}	Polymer electrolyte membrane	[168]
PVdF-g-tBA	PVdF	20 kV, 15 cm	Polymer electrolyte membrane	[169]
PVdF	PVdF	21 kV	Polymer electrolyte membrane	[179]
PVdF/PAN	PVdF, PAN	25 kV, 20 cm, 10 mL h^{-1}	Polymer electrolyte membrane	[173]

Table 3 (*Continued*)

Materials	Precursors	Electrospinning parameters	Applications	References
PVdF/OC/TPGDA	PVdF, OC, TPGDA	15 kV, 15 cm	Polymer electrolyte membrane	[174]
PPy/SEBS	Ppy, SEBS, Super-P	20 kV, 18 cm, 1 mL h^{-1}	Polymer electrolyte membrane	[182]
TiO_2	Titanium tetraisopropoxide	10 kV, 0.3 mL h^{-1}	Pt catalyst support	[62]
TiO_2	Titanium (IV) n-butoxide, PVP	15 kV	Photoelectrode for DSSC	[94]
TiO_2	Titanium (IV) isopropoxide, PVP	30 kV, 10 cm, 2 mL h^{-1}	Photoelectrode for DSSC	[81]
TiO_2	Titanium (IV) propoxide, PVAc	15 kV, 10 cm, 60 μL min^{-1}	Photoelectrode for DSSC	[80,95–98]
TiO_2	Titanium iso-propoxide, PVP	14 kV, 7 cm, 0.8 mL h^{-1}	Photoelectrode for DSSC	[99]
TiO_2	Titanium (IV) isopropoxide, PVP	10 kV, 10 cm, 1 mL h^{-1}	Photoelectrode for DSSC	[100]
TiO_2	Titanium (IV) butoxide	15 kV, 15 cm	Photoelectrode for DSSC	[88]
TiO_2	Titanium isopropoxide, PVAc	20 kV, 14 cm	Photoelectrode for DSSC	[102]
TiO_2	Titanium (IV) isopropoxide, PVP	1.2 kV cm^{-1}, 0.8 mL h^{-1}	Photoelectrode for DSSC	[103]
TiO_2	Titanium n-propoxide, PVAc	12–15 kV, 10 cm, 30 μL min^{-1}	Photoelectrode for DSSC	[104]
TiO_2	Tetra-n-butyl titanate, PVP, MWCNT	30 kV, 15 cm	Photoelectrode for DSSC	[106]
TiO_2	Titanium (IV) isopropoxide, PVP	30 kV, 2 mL h^{-1}	Anode for Li-ion battery	[162]
ZnO	Zinc acetate, PVAc	15 kV, 10 cm,, 15 μL min^{-1}	Photoelectrode for DSSC	[108]
ZnO	Zinc acetate, poly(ethylene oxide)	0.6 kV cm^{-1}, 0.5 mL h^{-1}	Photoelectrode for DSSC	[109]
V-ZnO	Zinc acetate, vanadyl acetylacetonate, PVP, ethanol and water	21 kV, 16 cm, 0.03 mL min^{-1}	Piezoelectric material	[205,206]
Co_3O_4	Cobalt acetate, citric acid	25 kV, 30 cm	Anode for Li-ion battery	[164]
Co_3O_4	Cobalt nitrate, PVP	20 kV, 15 cm	Anode for Li-ion battery	[165]
NiO/SWCNT	$Ni(CH_2COO)_2{\cdot}4H_2O$, PVP, SWCNT	20 kV, 20 cm	Anode for Li-ion battery	[155]
NiO/P(VdF-HFP)/C	NiO, P(VdF-HFP), acetylene black	15 kV, 15 cm, 1 mL h^{-1}	Electrode for supercapacitor	[194]
PVP/$RuL_2(NCS)_2$,TiO_2	PVP, $RuCl_3{\cdot}3H_2O$, 4,4′-dicarboxy-2,2′-bipyridine, titanium isopropoxide	15 kV, 25 cm	Photoelectrode for DSSC	[114]
$LiCoO_2$	Lithium acetate, cobalt acetate, citric acid	25 kV, 30 cm	Cathode for Li-ion battery	[124]
$LiCoO_2$	Lithium chloride, cobalt acetate, PVA	12 kV	Cathode for Li-ion battery	[125]
$LiCoO_2$	$Co(C_2H_3O_2)2{\cdot}4H_2O$, Li(OiPr), PVP	1.2 kV, 2 cm	Cathode for Li-ion battery	[126]
$LiCoO_2$/MgO	Magnesium acetate, citric acid, lithium acetate, cobalt acetate	25 kV, 30 cm, 0.02 and 0.3 MPa (N_2)	Cathode for Li-ion battery	[129]
$LiNi_{1/3}Co_{1/3}Mn_{1/3-x}Al_xO_2$	Lithium nitrate, nickel nitrate, cobalt nitrate, manganese nitrate, aluminum nitrate, PVP	25 kV, 15 cm	Cathode for Li-ion battery	[132]
$LiFePO_4$/C	$LiNO_3$, $Fe(NO_3)_3{\cdot}9H_2O$, $NH_4H_2PO_4$, poly acrylic acid and MWCNTs	25 kV	Cathode for Li-ion battery	[135]
$SrRuO_3$–RuO_2	Ruthenium (III) chloride, PVAc, strontium (II) chloride hexahydrate	12–15 kV, 15 cm, 10 μL min^{-1}	Electrode for supercapacitor	[199]

Table 3 (*Continued*)

Materials	Precursors	Electrospinning parameters	Applications	References
Perovskite lead zirconate titanate (PZT)	Lead acetate trihydrate, zirconium (IV) n-propoxide, titanium (IV) isopropoxide, 2-methoxyethanol, acetic acid, PVAc methanol, ethanol	17 kV, 17 cm	Piezoelectric material	[201]
PZT	PZT (52/48) sol–gel, PVP	10 kV	Piezoelectric material	[202]
PZT	PZT (52/48) sol–gel, PVAc	10 kV, 15 cm, 0.05 mL h^{-1}	Piezoelectric material	[203]
$Bi_{3.15}Nd_{0.85}Ti_3O_{12}$	Bismuth nitrate, neodymium nitrate, titanium butoxide, PVP, glacial acetic acid, 2-methoxyethanol and DMF	32 kV, 16 cm	Ferroelectric materials	[204]
$NaCo_2O_4$	Sodium acetate trihydrate, cobalt (III) acetate tetrahydrate, polyacrylonitrile and DMF	20 kV, 10 cm, 1 mL h^{-1}	Thermoelectric materials	[207]
$Ca_3Co_4O_9$	Calcium acetate monohydrate, cobalt acetate tetrahydrate, PVP methanol and propionic acid	1.4 kV cm^{-1}, 0.015 mL min^{-1}	Thermoelectric materials	[211]

Table 4
Surface characterization of XC-72R and electrospun CNF (from Ref. [65]).

Sample	SSA (m^2 g^{-1})	V_{micro} (cm^3 g^{-1})	V_{meso} (cm^3 g^{-1})	V_{tot} (cm^3 g^{-1})	S_{micro} (m^2 g^{-1})	S_{meso} (m^2 g^{-1})	APD (nm)	Conductivity (S cm^{-1})
XC-72R	235	0.062	0.578	0.640	156	79	10.92	4.5
e-CNF	307	0.128	0.054	0.182	292	15	2.36	9.9
Pt/XC-72R	194	0.049	0.550	0.599	132	62	14.28	–
Pt/e-CNF	302	0.125	0.053	0.178	288	14	2.31	–

polymers such as polyaniline nanofibers (PANI) has been explored as an alternative for supporting the Pt nanoparticles [61]. A good support material must have a high surface area to disperse the nanoparticles over, large pores to allow gas flow and good electrical conductivity. PANIs have porous network structures and good electrical conductivity that can meet these requirements. Xia and coworkers [62] electrospun anatase nanofibers onto TiO_2 followed by Pt nanoparticles of 2–5 nm in size and varying densities of surface coverage. They reported higher electrochemical activity and durability for their supported Pt nanostructures for direct methanol oxidation compared with commercial Pt/C catalysts. Because of their high electrical conductivity, carbon nanofibers (CNFs) are also a promising fuel cell catalyst support material [57,63–67]. Park et al. [65] prepared CNFs by electrospinning and carbonization (Fig. 7). Unlike commercial XC-72R, these electrospun CNFs had high surface area, high electrical conductivity (Table 4) and shallow pores with rough surfaces. These properties can increase Pt utilization through an enhancement of the three-phase boundary. In addition to pure CNF, nickel nitrite doped CNFs created by electrospinning have been developed by Nataraj et al. [66]. Fig. 8 illustrates the presence of nickel nanoparticles in the CNFs. They reported that the surface characteristics of PAN-based CNFs increased significantly with 5 wt% nickel nitrite loading. Xuyen et al. [67] developed an immobilization process induced by hydrolysis to deposit Pt nanoparticles on the surface of polyimide (PI) based carbon nanofibers. Li et al. [68] thermally treated the electrospun polyacrylonitrile fibrous mats to get carbon fibrous mats (CFMs), and their tests showed that the commercial Pt/C supported on the CFMs exhibited higher electrocatalytic activity, more stability, larger exchange current and smaller charge transfer resistance. Since CNF surfaces are smooth and chemically inert, harsh oxida-

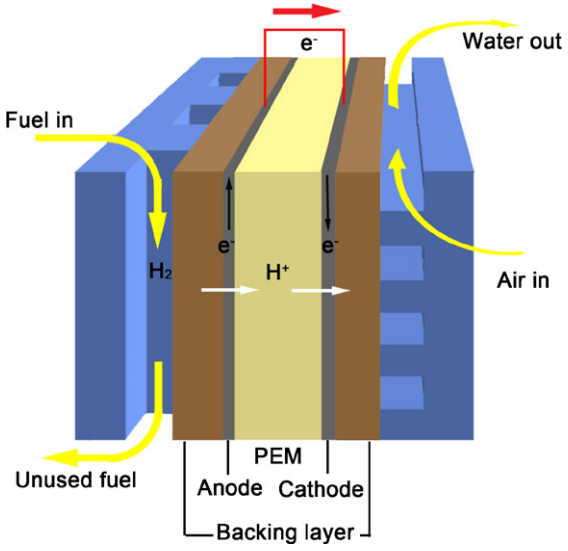

Fig. 5. Diagram of PEM fuel cell.

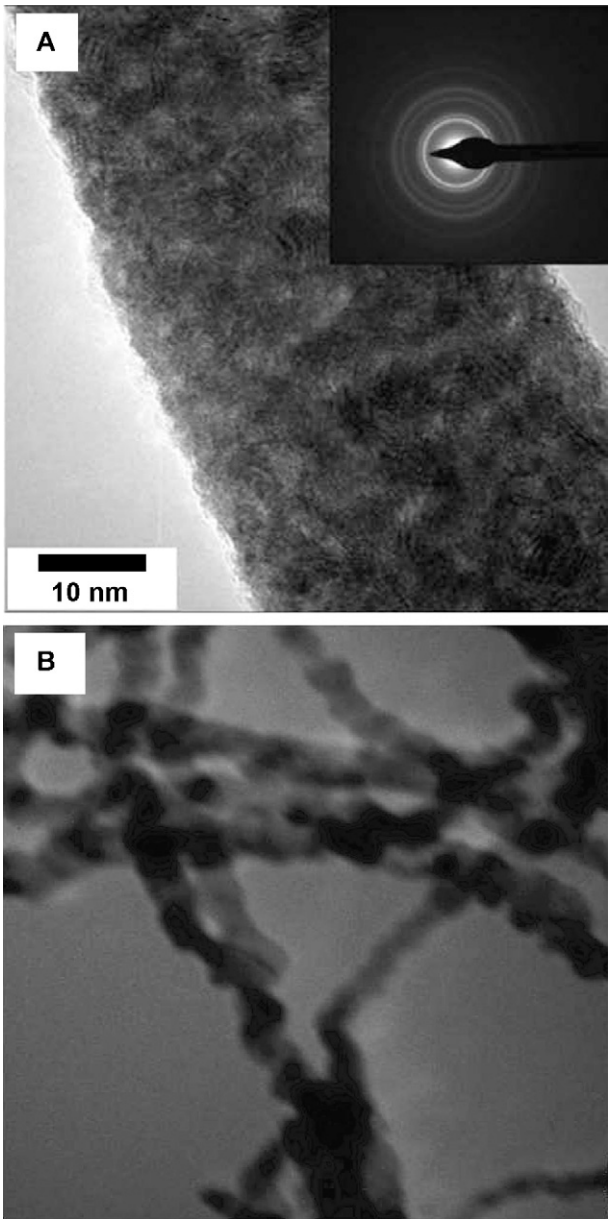

Fig. 6. (A) HRTEM image of a single nanowire Pt_1Rh_1 (from Ref. [50]); (B) TEM image of Pt nanowires (from Ref. [51]).

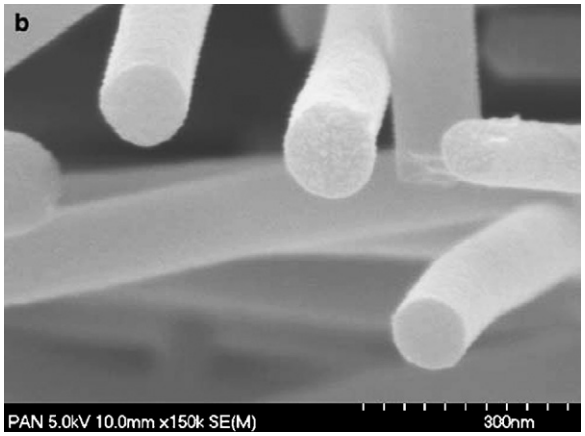

Fig. 7. SEM images of cross sections of electrospun CNF carbonized at 1000 °C (from Ref. [65]).

tive methods are usually used to produce active sites to get catalyst nanoparticles to deposit on and anchor to the surface of CNFs. Lin et al. demonstrated a mild functionalizing method to activate electrospun CNFs [69]. Pt is easier to deposit on the treated CNFs and the resulting catalyst material showed improved methanol oxidation performance and good long-term stability.

Electrospun CNFs are expected to play an important role as catalyst support structures in fuel cells. To mitigate potential CO poisoning risks and reduce cost, binary or ternary Pt-based catalysts have attracted significant attention. One such effort involves a gold coated electrospun CNF membrane that was prepared for Pt catalyst support [70]. The obtained Pt/Au-PAN membrane exhibited high electrocatalytic activity and stability while oxidizing methanol. Huang et al. [71] used electrospun CNFs to support PtAu bimetallic nanoparticles. The catalyst showed improved electrocatalytic activities and better CO tolerance. Besides CNFs, other materials can be used as supporting matrices. Su et al. [72] electrospun polyamide 6 (PA6) to make a catalyst support matrix and then deposited Pd on the surface of the PA6 nanofibers by the electroless plating method. This catalyst showed high current density and a low peak current ratio of the backward to forward scan (I_b/I_f), and may be used as freestanding electrocatalytic electrodes in direct methanol fuel cells. Hong et al. [73] prepared Pt loaded polystyrene membranes by electrospinning. The resulting in situ metalized Pt can also be used as a fuel cell catalyst.

3.1.3. Proton exchange membrane

The proton exchange membrane is the central element of a PEM fuel cell. To function, the membrane must absorb water and conduct hydrogen ions (protons), but not electrons or gas. It also should have sufficient mechanical strength to withstand normal operation. Membranes made of Nafion can provide a continuous path for proton ion flow, however, Chen et al. [74] studied the electrospinning performance and solution properties of Nafion and its blend with poly(acrylic acid) (PAA). They found that pure Nafion is not a good candidate for electrospinning because of its low viscosity. Nafion solutions must be mixed with other polymers to suppress aggregate formation and increase viscosity for proper electrospinning. Besides PAA, other polymers such as polyethylene oxide (PEO), polyvinyl alcohol (PVA) and polyvinyl pyrrolidone (PVP) were also used to make a spinnable Nafion/polymer solution [75]. Results showed PVP/alcohol had the best compatibility with Nafion/Nafion-PTFE and the surface finish of the obtained fibers was smooth. To overcome the high crossover of methanol fuel in direct methanol fuel cells, Choi et al. [76] made composite membranes consisting of electrospun polyvinylidene fluoride (PVdF) and different amounts of Nafion. Although PVdF has lower proton conductivity than Nafion membranes, its tortuous framework structure helps to reduce the methanol crossover. A Nafion/PVdF composite membrane maintains the unique three dimensional network structure of PVdF and exhibits better performance than a Nafion 115 membrane in direct methanol fuel cells (DMFC). Chen et al. also investigated PVdF and PVdF/phosphotungstic acid (PWA) membranes [77]. They found that adding PWA could eliminate the formation of beads in the electrospun fibers, and change the PVdF crystal phase from α- to β-phase. Recently, a composite membrane containing uniaxially aligned sulfonated polyimide nanofibers was fabricated via electrospinning [78]. This membrane exhibited high proton conductivity, low gas permeability, good chemical resistance and thermal stability.

3.2. Dye-sensitized solar cells

Electrospun materials can also be used in the manufacturing of solar cells. Solar cells convert the energy of sunlight directly into electrical energy via the photovoltaic effect. Solar cell develop-

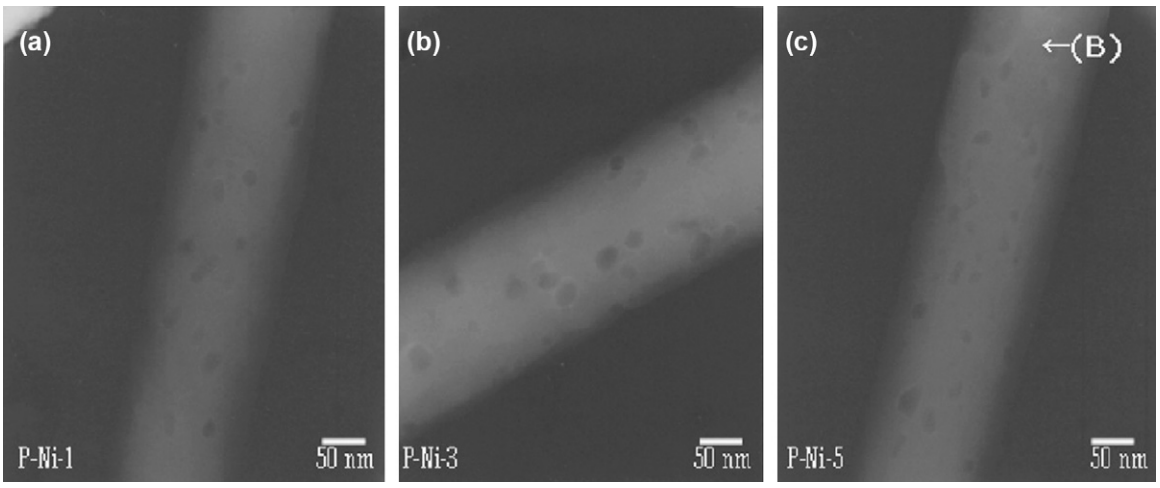

Fig. 8. TEM images of CNFs with (a) 1 wt%, (b) 3 wt% and (c) 5 wt% nickel nitrate incorporated and carbonized at 1000 °C in N_2 atmosphere (from Ref. [66]).

ment has progressed through several stages including crystalline silicon, thin-film and now a third generation of solar cells, dye-sensitized solar cells (DSSC), which covers a variety of advanced thin-film technologies. Dye-sensitized solar cells are a relatively new class of thin-film solar cells. They were invented by Oregan and Gratzel [79] in 1991 and received a great deal of attention for their low cost and ease of manufacturing. DSSC technology can be described as an "artificial photosynthesis" process. In the original Gratzel design, a cell was composed of three main parts; a transparent fluorine-doped tin oxide (SnO_2:F) deposited on a glass plate served as the anode, a platinum sheet was the cathode, and a photosensitive ruthenium-polypyridine dye deposited TiO_2 (or ZnO, etc.) film with a thin layer of iodide was sandwiched between the two electrodes. Fig. 9 is a schematic illustration of DSSC. The use of electrospun materials in DSSC photoelectrodes and electrolytes is discussed in depth in some publications [80–82].

3.2.1. Photoelectrode

In a DSSC, the dye on a TiO_2 surface collects solar energy and loses an electron to the conduction band of the TiO_2. From there it moves to a clear anode by diffusion and then to an external circuit. Various titania films have been made by methods such as spin coating [83–85], screen-printing [86], and doctor blading [83]. However, the electron diffusion coefficient of nanoparticles is more than two orders of magnitude less than that of bulk anatase crystals [87]. These particle-based titania layers have low efficiencies due to the high density of grain boundaries which exist between nanoparticles. The 1D morphology of metal oxide fibers attracts more interest because of the lower density of grain boundaries compared to those of sintered nanoparticles [80,88].

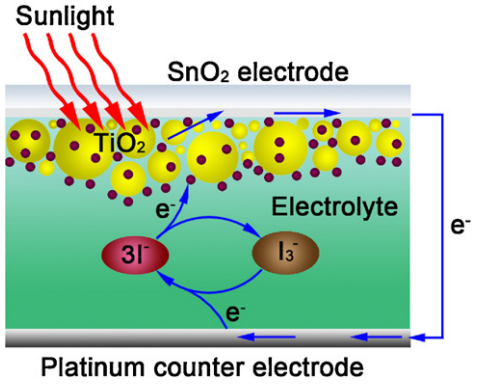

Fig. 9. Scheme of dye sensitized solar cell.

Electrospun nanofiber anodes can offer high specific surface areas (ranging from hundreds to thousands of square meters per gram) and bigger pore sizes than nanoparticle or film anodes. This is because the electrolyte used in DSSCs usually consists of triiodide/iodide redox coupled in organic solvents. Additionally, the liquid electrolytes within DSSCs lack long-term stability [89]. To overcome these problems, many solid or semi-solid electrolytes were investigated, such as inorganic or organic hole conductors [90], ionic liquids [91], polymers [92], and gel electrolytes [93]. However, solid or semi-solid electrolytes are too viscous to sufficiently penetrate the TiO_2 layer. Nanofiber anodes with large and controllable pore sizes may increase the penetration of viscous polymer gel electrolytes. A detailed investigation of the morphological and structural properties of several as-electrospun precursor nanofibers and the resulting final TiO_2 nanofibers was conducted by Chandrasekar et al. [94]. Results showed that all final TiO_2 nanofibers were composed of anatase-phased TiO_2 single-crystalline grains. Fig. 10 shows the TEM image and electron diffraction pattern (insets) of the electrospun TiO_2 nanofibers. Mukherjee et al. investigated electron transport within electrospun TiO_2 nanofibers [81]. The cells exhibited high effective electron diffusion coefficients but low electron lifetimes. Song and Jo et al. [80,95–98] also developed nanofiberous titania thin-film layers via electrospinning. These electrospun titania nanofibers have larger pores, which increase the penetration of viscous polymer gel electrolyte. The observed solar–electric energy conversion efficiency from the electrospun TiO_2 electrodes with poly(vinylidenefluoride-co-hexafluoropropylene)(PVDF–HFP) gel electrolytes was over 90% of that from a liquid electrolyte system.

In addition to randomly oriented nanofibers, TiO_2 nanowires have been electrospun in an aligned orientation. By cross-aligning TiO_2 nanowires, the electrical resistance can be reduced by 30% and the solar cell performance can be enhanced by 70% [99]. Fig. 11 shows the morphology of (A) uniaxially aligned and (B) cross-aligned TiO_2 nanofibers on a flat substrate.

TiO_2 can exhibit poor adhesion to substrates after calcination. To address this, some research groups have developed new treatment methods for the photoelectrode. A TiO_2 electrode consisting of a nanoparticle/nanorod layer was prepared by mechanically grinding electrospun TiO_2 nanofibers to nanorods, then spraying and sintering them on a conductive glass plate [100]. An energy conversion efficiency of about 5.8% was reported for this electrode. Mechan-

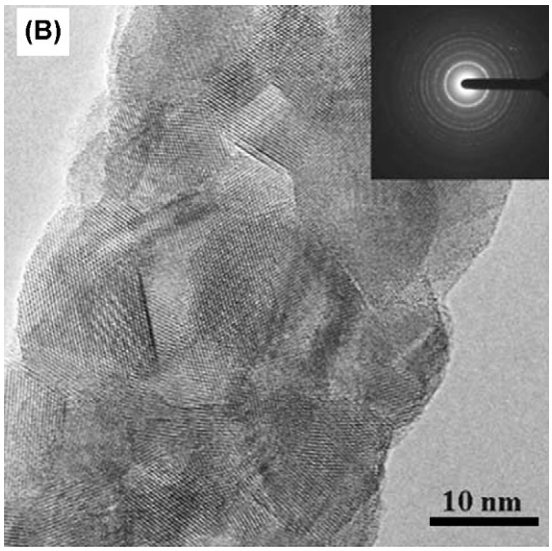

Fig. 10. TEM image and electron diffraction pattern (inset) of electrospun TiO_2 nanofibers made from titanium (IV) n-butoxide, PVP, and DMF/isopropanol (1/1 mass ratio) mixture (from Ref. [94]).

ically grinding TiO_2 nanofibers to nanorods increases the number of grain boundaries which lowers the conversion efficiency [88] while nanowire/nanoparticle composites offer both rapid electron transport rates and high surface areas [101]. Recently, a composite anatase TiO_2 nanofibers/nanoparticle electrode was fabricated

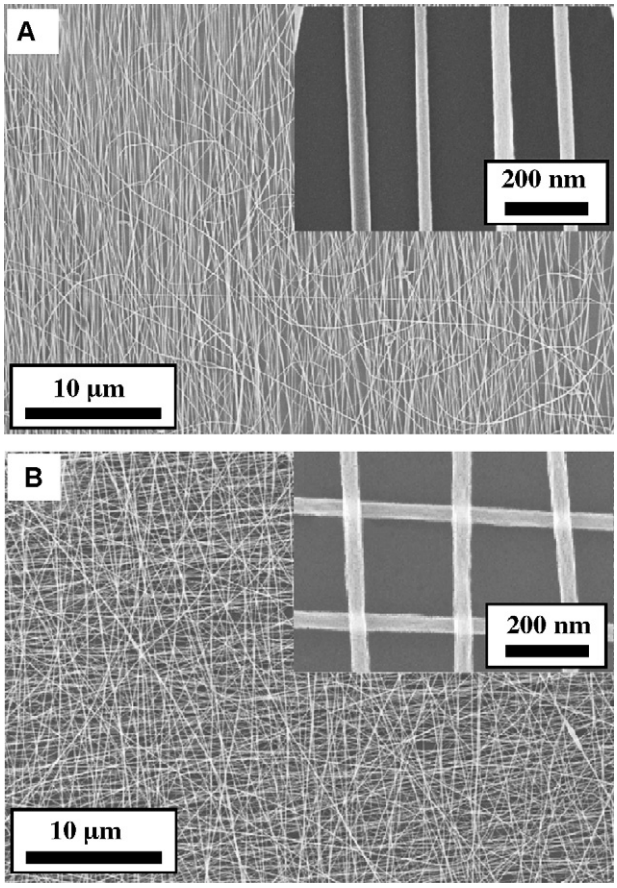

Fig. 11. SEM images of (A) uniaxially-aligned and (B) cross-aligned TiO_2 NWs on a flat substrate. Inset figures display enlarged SEM images of each sample (from Ref. [99]).

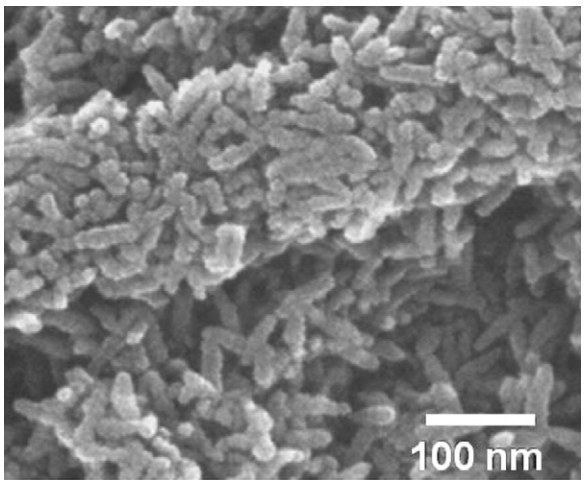

Fig. 12. SEM images of electrospun TiO_2-nanorod nanofibers after calcination at 400 °C (from Ref. [104]).

through electrospinning [88]. This method avoided the mechanical grinding process, and offered a higher surface area, so conversion efficiencies of 8.14% and 10.3% for areas of 0.25 and 0.052 cm^2, respectively, were reported.

Performance can also be improved by increasing the adhesion between the deposited nanofibers and the substrate. Onozuka et al. [102] applied an additional adhesion treatment to their predeposited TiO_2 film using DMF in their Ru(II)-sensitized solar cells. Also investigated was an ultra-thin surface treatment, used as a binding layer in a hybrid photovoltaic device, that still requires further improvements to reach higher efficiency [103]. Lee et al. synthesized TiO_2 nanorod (NR)-based electrodes by electrospinning [104]. Fig. 12 shows that after calcination, the TiO_2 nanofibers were composed of many TiO_2 nanorods. These nanorods had a relatively low number of defects and fewer grain boundaries, so there were fewer electron trapping events, and therefore, longer recombination lifetimes [105]. This electrode exhibited higher energy conversion efficiencies than nanoparticle electrodes. $TiCl_4$ post-treatment improved the electron diffusion coefficient further [104]. Hybrid TiO_2 nanofibers with moderate MWCNT content also can prolong electron recombination lifetimes [106]. Since MWCNTs can quickly transport charges generated during photocatalysis, the opportunity for charge recombination is reduced. Furthermore, MWCNTs decrease the agglomeration of TiO_2 nanoparticles and increase the surface area of TiO_2. These advantages make this hybrid electrode a promising candidate for DSSCs.

While DSSCs utilizing nanocrystalline TiO_2 are under intensive investigations, ZnO has proven to be another promising photoelectrode material due to its similar band gap and comparable electron injection process as that of TiO_2 [107]. A convenient method to fabricate nanofibrous ZnO photoelectrodes by electrospinning has been reported [108]. The electrospun ZnO nanofibers had a dense, twisted structure of 200–500 nm diameter cores with ~30 nm single grains. This structure offered high surface area, high porosity for efficient electrolyte penetration and direct conduction paths. These structure morphologies resulted in a cell that had a conversion efficiency of 1.34% under 100 mW cm^{-2} illuminations. Zhang et al. applied a $Zn(OAc)_2$, treatment to electrospun ZnO nanofibers [109]. The resulting nanofibers had tunable thicknesses, good adhesion to FTO substrates and yielded a DSSC with an energy conversion efficiency of 3.02%. Although this conversion efficiency is lower than TiO_2 cells, it is still a great improvement over existing ZnO DSSCs [110–113]. In addition to inorganic electrodes, electrospinning has been used to make an organic/inorganic composite electrode [114]. This electrode, made from a PVP, $RuL_2(NCS)_2$ and a TiO_2 nanoparti-

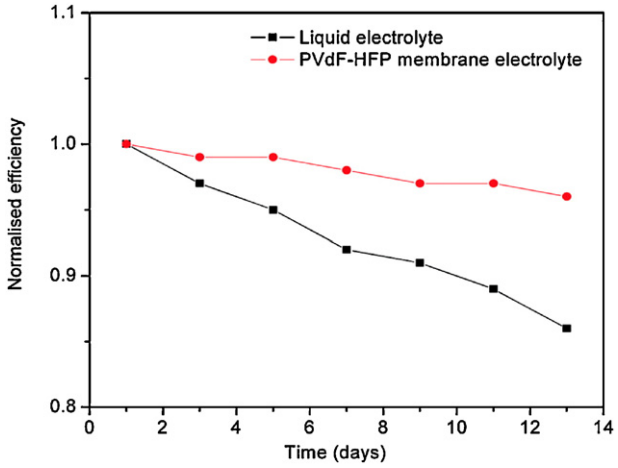

Fig. 13. Normalized DSSC light-to-electricity conversion efficiency variation over time for liquid electrolyte and electrospun PVdF-HFP membrane electrolyte (from Ref. [82]).

cle mixture, may bring the advantages of both organic and inorganic materials to DSSCs. Recently, indium tin oxide (ITO) nanofiber film prepared by electrospinning was reported [115]. The film, composed of electrospun fibers with average diameters of 200 nm, successfully adhered to glass. The resulting 16.76% improvement in the conversion efficiency was attributed to the reduction of grain boundaries.

3.2.2. DSSC electrolyte

As previously discussed, the traditional liquid electrolytes within DSSCs have poor durability, so many solid or semi-solid electrolytes have been used in DSSCs. Quasi-solid-state or gel polymer electrolytes are desirable because of their long-term stability. To make the best of these electrolytes, a good design requires the consideration of the resulting electrolyte stability and encapsulation. Electrospun polymer membranes have inter-connected pores, which help to encapsulate electrolyte solution. Priya et al. prepared a PVdF-HFP membrane by electrospinning from a solution of poly(vinylidenefluoride-co-hexafluoropropylene) in a mixture of acetone/N,N-dimethylacetamide. Although the solar energy-to-electricity conversion efficiency of the quasi-solid-state solar cells with the electrospun PVdF-HFP membrane was slightly lower than the value obtained from the conventional liquid electrolyte solar cells, this cell exhibited better long-term durability because of the prevention of electrolyte solution leakage [82]. Fig. 13 shows the conversion efficiency of liquid electrolyte as it decreased over time, whereas that of the quasi-solid-state solar cells remained at 96% of its initial value. Similar work was done by Park et al. [116] and Kim et al. [117]. They found the photovoltaic performance of DSSC devices using electrospun PVDF-HFP nanofiber films was much better than that observed from spin-coated PVDF-HFP films.

3.3. Lithium-ion batteries

Lithium-ion batteries (sometimes abbreviated Li-ion batteries) are a type of compact, rechargeable power storage device with high energy density and high discharge voltage. They are established market leaders in clean energy storage technologies because of their relatively high energy-to-weight ratios, lack of memory effect and long life [118]. Typically, lithium-ion batteries consist of three primary functional components: an anode, a cathode, and an electrolyte (Fig. 14), for which a variety of materials may be used. There are opportunities for electrospinning to create new materials that potentially improve all three of these components.

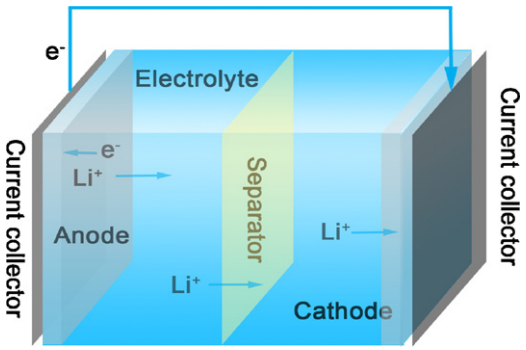

Fig. 14. Schematic illustration of a Li-ion battery.

3.3.1. Cathode materials

In 1991, Sony produced the first commercial lithium-ion battery. Sony used a layered oxide (such as lithium cobalt oxide) as a cathode material. Later, manganese spinel-based Li-ion batteries were introduced by Goodenough and coworkers [119]. Today, lithium iron phosphate ($LiFePO_4$) and other phospho-olivines are the most popular cathode materials; however, all of these material types are still under investigation. The layered oxide $LiCoO_2$ has high specific energy density, low self-discharge and excellent cycle life [120,121], so it attracts a great deal of interest as a cathode material. One drawback of this electrode material is the slow solid state diffusion of Li^+ cations within them [122,123]. Nanofiber materials may offer an opportunity to resolve this problem because of their shorter diffusion distances for Li^+ cations. Gu et al. [124] developed a $LiCoO_2$ fiber cathode by combining a sol–gel method with electrospinning. Fig. 15 shows that while this cathode had a high initial discharge capacity of 182 mAh g^{-1}, this value decreased rapidly to 123 mAh g^{-1} after 20 cycles. Electrospun $LiCO_2$ nanofibers have also been obtained from a PVA/lithium chloride/cobalt acetate/water solution. After calcination treatment, the resulting $LiCoO_2$ fibers had diameters of 100–150 nm [125]. Lu et al. also electrospun $LiCoO_2$ fibers and investigated their structural stability and electrochemical performance [126]. Results showed that a coating of lithium phosphorous oxynitride could improve the structural stability and cyclability. Making core–shell structured nanofibers with metal oxide shells to protect the $LiCoO_2$ may be an effective way to maintain its structural stability [127,128]. Gu et al. [129] introduced a procedure to make $LiCoO_2$ nanoparticle core, amorphous MgO shell coaxial fibers by co-electrospinning.

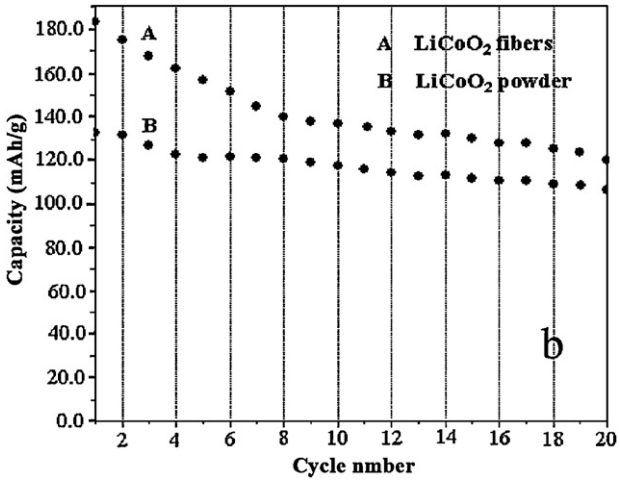

Fig. 15. Cycle life of the $LiCoO_2$ fiber and powder electrodes at a current density of 20 mAh g^{-1} (from Ref. [124]).

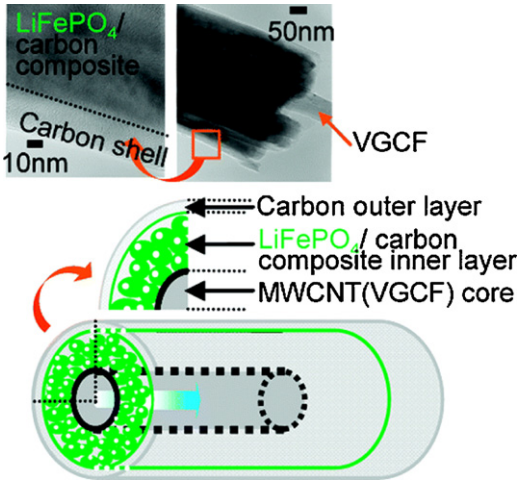

Fig. 16. TEM image and diagram of the triaxial nanowire with a MWCNT core column, and the two layer shells of Si/C fibers (from Ref. [135]).

Characterization of the fiber indicated that the MgO shell prevented the impedance growth and resulted in a fiber with good cyclability. Although $LiCoO_2$ has good recharge ability, it also has drawbacks such as high cost and toxicity. For this reason, $LiNi_{1/3}Co_{1/3}Mn_{1/3}O_2$, which has the same layered structure as $LiCoO_2$, has been considered as an alternative cathode material [130,131]. Partial substitution is an effective method to improve the electrochemical properties of $LiNi_{1/3}Co_{1/3}Mn_{1/3}O_2$. Recently, $LiNi_{1/3}Co_{1/3}Mn_{1/3-x}Al_xO_2$ ($0 \le x \le 0.08$) nanofibers were fabricated by electrospinning [132]. Results showed that aluminum doping resulted in noticeable improvement in the electrochemical performance, especially at $x = 0.06$.

Lithium-transition-metal-oxide, $LiMnO_2$, is another high performance cathode material that can be used in lithium-ion batteries. Sun et al. [133] prepared manganese oxide nanofibers via the calcination of electrospun composite nanofibers. The results showed a high reversible discharge capacity of 160 mAh g^{-1} that was maintained at about 132.5 mAh g^{-1} after 50 cyclings. The structural stability of manganese oxide nanofibers was also confirmed by SEM.

As was previously discussed, $LiFePO_4$ is a commonly used cathode material; however, its low electron conductivity motivates researchers to continue to look for better solutions. Currently, carbon coating is an effective method for improving the electrical conductivity of $LiFePO_4$ [134]. A triaxial $LiFePO_4$ nanowire has been electrospun from a composite precursor solution. The nanowire includes a MWCNT core, an amorphous carbon outer shell, and an $LiFePO_4$/amorphous carbon composite layer between them as illustrated in Fig. 16 [135]. The authors reported that the carbon core and the outer layer played an important role in forming an electrical conduction pathway.

3.3.2. Anode materials

The most popular anode material in commercially available lithium-ion batteries is carbon. Either hard carbon or graphite is used to ensure stable capacity during cycling. However, the theoretical capacity of graphite is very limited, only 372 mAh g^{-1} [136]. In contrast, silicon has the highest known theoretical capacity at 3572 mAh g^{-1} [137] at room temperature, but poor cycling stability. One of the most promising ways to improve the cyclability of silicon is by making Si/C composites that have stable structures and good electroconductivity. Ji and Zhang [138,139] made Si nanoparticle-loaded porous carbon (C/Si) nanofibers by electrospinning polyacrylonitrile (PAN)/poly-L-lactic acid (PLLA)/Si composite nanofibers, which were then treated by stabilization (in air) and carbonization (in argon). Fig. 17(A) shows the morphology of heat-treated C/Si fibers. Electrochemical tests revealed high reversible capacity and relatively good cycling performance at high current densities. Similar work was also done by Fan et al. [140]. In their work, nano-Si/C composites were fabricated simply by the carbonization of electrospun Si/Poly(vinyl alcohol) (PVA) composite nanofibers. The resultant Si/C composite nanofiber anodes exhibited a gradual increase in capacity as it was cycled, reaching 892.5 mAh g^{-1} after 50 cycles.

Like silicon, transition metal oxides also have high theoretical capacity. However, also like silicon, transition metal oxides suffer from poor cycling performance [141] due to their mechanical instabilities. Incorporating nano-sized transition metal oxides into porous carbon nanofibers (CNFs) is a promising method for overcoming these problems. Wang et al. [142] prepared C/Fe_3O_4 composite nanofibers by electrospinning PAN/Fe_3O_4 compounds which were then pyrolysized. Electrochemical characterization showed the C/Fe_3O_4 composite nanofibers obtained at 600 °C had high reversible capacity, good cycling performance and excellent rate capability. Another carbon based composite, C/MnO_x, was used to create a nanofiber anode via the electrospinning technique followed by thermal treatments in different environments [143,144]. Since MnO_x can exhibit high capacity and the stable porous composite fibers had high surface area, the combinative effects resulted in a material with a high reversible capacity, long cycle life, and good rate capability.

Transition metals can also be used to make carbon-based composite anodes; their good electrical conductivity can create an electronic pathway in electrodes to enhance electrochemical performance [145]. Ji et al. made C/Ni [146] and C/Cu [147] composite fibers via electrospinning. The obtained electrodes exhibited good electrochemical performance including large reversible capacity, improved cycle performance, and better rate capacity. Yu et al. demonstrated C/Sn composites with core–shell structure [148,149]. Single-crystal metallic tin was encapsulated in amorphous multichannel carbon microtubes and "bamboo-like" hollow carbon nanofibers (Fig. 17(B)). The encapsulated tin particles shorten the transport lengths for both electrons and lithium ions, and the hollow carbon nanofibers offer good contact between electrode and electrolyte. These electrodes showed good electrochemical performance especially in reversible capacity. Non-woven C/Sn film has also been prepared by electrospinning [150]. Tin particles were homogeneously dispersed in carbon fibers. The reversible capacity of the film was at 96.7% of its original value after 20 cycles. Wang et al. have electrospun C/Co nanofibers. The embedded Co can increase the interfacial surface area between the carbon and liquid electrolyte and enhance the electrical conductivity. This composite fiber exhibited high conductivity, large reversible capacity and good cyclability [151].

Nanosized NiO is also a potential anode material for Li-ion batteries [152] and researchers have directed a great deal of effort into investigating its electrochemical properties [153,154]. Recently, Lu et al. proposed a new method to synthesize single-wall carbon nanotube (SWCNT) reinforced NiO fibers through electrospinning. Because SWCNTs can improve mechanical strength and electrical conductivity, this NiO/SWCNT electrode exhibited good rate capacity and cyclability [155]. In addition to these in situ synthesized composite fibers, another C/Mn_3O_4 composite anode was fabricated by mixing and hot-pressing carbon black and Mn_3O_4 fibers [156]. An electrochemical capacity of 450 mAh g^{-1} for at least 50 cycles can be obtained from this electrode.

Ji et al. [157–159] have synthesized porous CNFs using electrospinning. The obtained carbon fibers had unique structural features such as high porosity, high surface area, numerous active sites, short diffusion pathways and reasonable electrical conduc-

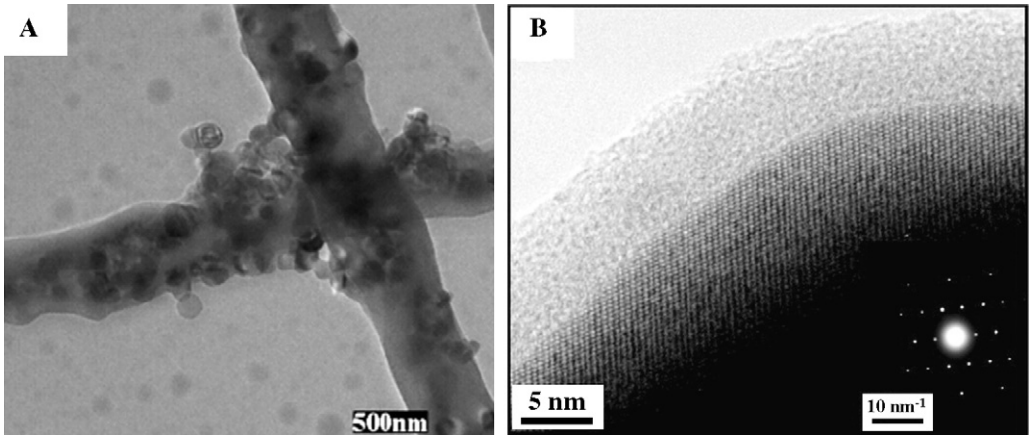

Fig. 17. (A) TEM image of Si/C fibers (from Ref. [139]); (B) HRTEM micrograph and SAED pattern of an isolated Sn nanoparticle, revealing the presence of single-crystalline metallic tin and amorphous carbon (from Ref. [148]).

tivity, which contributed to initial reversible capacities of about 566 mAh g^{-1} and 435 mAh g^{-1} after 50 cycles.

Besides these carbon related materials, anatase TiO_2 has also attracted considerable interest for its potential application in lithium-ion batteries [160,161]. Reddy et al. [162] synthesized anatase TiO_2 nanofibers by electrospinning and nanoparticles by the molten salt method. Electrochemical characterization showed that although electrospun TiO_2 nanofibers had lower specific capacity than TiO_2 nanoparticles, their electrochemical cycling stability was higher. These results indicate that TiO_2 nanofibers may be another potential anode material for lithium-ion batteries. Co_3O_4 is another possible anode material with high reversible capacity and electrochemical stability [163]. Gu et al. [164] and Ding et al. [165] prepared Co_3O_4 nanofibers by electrospinning. As expected, these Co_3O_4 nanofibers exhibited high reversible capacity and good cycle stability.

3.3.3. Polymer electrolytes

Because of their good chemical and mechanical stability, polymer electrolytes for Li-ion batteries have been widely investigated. Gel polymer electrolytes have high ionic conductivity and are easy to fabricate. However, the soft morphology of polymer electrolytes is not suitable for high speed processing. This has hindered their adoption in commercial lithium-ion batteries. PVdF homopolymer has high crystallinity (i.e., it is not too soft), so it may be a good choice to circumvent processing problems [166]. However, PVdF based gel polymer electrolyte exhibits low ionic conductivity and low stability, perhaps because its crystallinity may lower the migration rate of Li ions [167]. Nanoporous polymer has high porosity and an interconnected open pore structure, so the electrolyte solution can be easily encapsulated within the matrix. As a result, this structure can contribute to a high ionic conductivity, and with sufficient mechanical strength, may be more suitable for lithium-ion battery fabrication. Electrospinning is a simple, cost-efficient technique capable of fabricating such nanoporous polymer membranes.

Gao et al. [168] investigated the morphologies, thermal properties, crystal structure and electrospinning parameters of electrospun PVdF membranes. Cell performance was also tested, and better cycling ability and charge–discharge performance with little capacity loss were claimed. Choi et al. [167] fabricated PVdF electrospun membranes to serve as polymer electrolyte for lithium polymer batteries. This membrane had high porosity and interconnected pores so that Li ions could easily move through the pores in polymer matrix, which leads to high Li ion conductivity. Excellent physical and electrochemical properties were obtained.

Another method for lowering the crystallinity of PVdF is making suitable copolymers or modified PVdF. For example, poly(vinylidene fluoride)-graft-poly(tert-butyl acrylate) (PVDF-g-tBA) copolymer-based electrolyte membrane was fabricated by electrospinning [169]. In addition to the interconnected pores providing fast paths to ions, the graft copolymer also lowered the crystallinity, so the electrolyte exhibited better ionic conductivity, electrochemical stability, interfacial resistance and cyclic performance. Poly(vinylidenefluoride-co-hexafluoropropylene) (P(VdF-HFP)) copolymer is another commonly used polymer electrolyte host material because it can easily be swollen and wetted by electrolyte solution. Kim et al. [170] prepared microporous P(VdF-HFP)-based fibrous membranes by electrospinning. The resultant polymer electrolyte membranes showed a low level of leakage of electrolyte solution due to the high specific surface area, high porosity and good compatibility between P(VdF-HFP) and the electrolyte. An ionic conductivity higher than 1×10^{-3} S cm^{-1} at room temperature was obtained from this electrospun membrane. The incorporation of room temperature ionic liquid into polymer electrolytes is another effective method for improving the electrochemical stability and compatibility of Li metal electrodes. Kim et al. prepared ionic liquid-activated, electrospun P(VdF-HFP) as an electrolyte host. The use of ionic liquid resulted in better compatibility between the P(VdF-HFP) and the electrode while addressing safety concerns regarding the high vapor pressures and low flash points of other lithium polymer batteries. The battery also yielded improved cycle stability and higher discharge capacity [171]. To improve the physical properties and electrolyte affinity, P(VdF-HFP)/PMMA composite was also fabricated by electrospinning [172]. With the addition of PMMA, the crystallinity of PVdF-HFP decreased, so the uptake capability and ionic conductivity of the membrane were improved. The hard PMMA chains also enhanced the tensile strength of PVdF-HFP. To resolve the problem of dissolving PVdF in common liquid electrolytes, PVdF/PAN composite fibers were fabricated by electrospinning [173]. The obtained electrode had high ionic conductivity; furthermore, with the presence of PAN, the electrode also exhibited higher liquid electrolyte uptake and good stability. In addition to PVdF based copolymer, organomodified clay (OC)/tripropyleneglycol diacrylate (TPGDA) modified PVdF also showed improved mechanical properties because of the chemical crosslink [174]. That sub-micron sized ceramic fillers (like SiO_2, Al_2O_3, TiO_2) can improve the handling strength and ionic conductivity of polymer electrolyte has been well illustrated [175,176]. Kim et al. [177] made P(VdF-HFP)/SiO_2 composite membranes by electrospinning. Although the inclusion of ceramic filler resulted in less homogenous fibers, the composite membranes showed

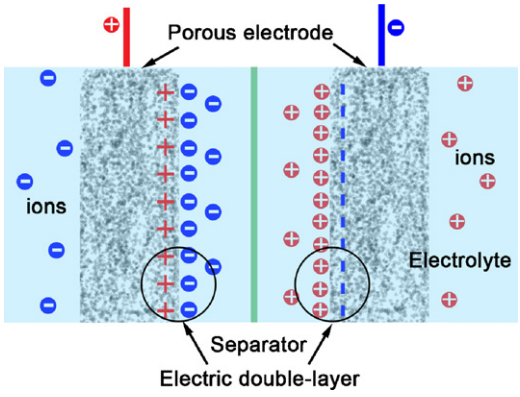

Fig. 18. Scheme of a supercapacitor.

higher ionic conductivities than membranes with the same porosity level but no SiO_2. However, mechanically mixed SiO_2 particles can aggregate. In order to overcome this problem, Raghaven prepared P(VdF-HFP)/in situ SiO_2 composite nanofibers by electrospinning [178]. With 6% in situ silica, this membrane showed the highest ionic conductivity.

To utilize non-aqueous electrolytes, a sandwiched polymer membrane was prepared by inserting one layer of PMMA film between two electrospun PVdF membranes [179]. The unique structure helps electrolyte uptake and ionic migration, and the results showed an ionic conductivity of 1.93×10^{-3} S cm^{-1}.

Polyacrylonitrile (PAN) is another common host polymer that can be used in the preparation of polymer electrolytes. It has high ionic conductivity, high thermal stability and good compatibility with electrolytes. A microporous polyacrylonitrile nonwoven membrane was electrospun by Cho et al. [180,181]. The PAN membranes showed higher ionic conductivities, higher retained capacities and better rate capabilities. Ju et al. [182] electrospun PPy/sulfonated SEBS nanofibers with the addition of sulfonated SEBS. This resulted in an improvement in the electrical conductivity of the composite fibers, and thus the electrochemical capacity was increased.

3.4. Supercapacitors

Supercapacitors, also known as electric double-layer capacitors, are novel high power density devices. Fig. 18 presents a schematic illustration of a supercapacitor. They have many advantages such as high power output and the ability to charge and discharge rapidly. Their capacitance depends on the surface area accessible to electrolyte ions, i.e., the pore size and porosity. Currently, commercial supercapacitors use porous carbon as electrodes, and porous carbon materials have been intensively studied [183–186]. Researchers, in order to improve the performance of supercapacitors, have put significant effort into the optimization of the structure of porous carbon materials. Electrospinning techniques can fabricate carbon membranes with high surface area with good control over pore size. Carbon nanofiber membranes have been synthesized via electrospinning from polybenzimidazol (PBI) [187,188]. PBI has good thermal and mechanical stability and good resistance to chemicals. Because of its rigid polymer chain, PBI does not require an additional stabilization process, which makes it an attractive candidate for carbon nanofiber membranes. The PBI carbon nanofibers obtained by Kim et al. had average diameters of 250 nm and a surface area of 500–1220 m^2 g^{-1}. The capacitor exhibited specific capacitance ranging from 35 to 202 F g^{-1}.

Kim et al. also prepared electrospun carbon nanofiber membranes from PAN, with [189] and without [190] the presence of zinc chloride, and also from PAA [191]. The sample with zinc chloride was stabilized in an air atmosphere at 280 °C for 1 h, sintered at 800 °C for 1 h in argon and washed in acid and DI water, which yielded black conductive carbon membrane. The membrane had an average fiber diameter of about 100 nm and surface area of 310–550 m^2 g^{-1}. The results also showed that PAN membranes with 5% zinc chloride led to the highest capacitance. The sample without zinc chloride was stable in a 6 M KOH solution, and exhibited surface area and capacitance of 460–1160 m^2 g^{-1} and 91–134 F g^{-1} respectively. The CNF obtained from PAA also had similar properties (a specific surface area of 1450 m^2 g^{-1} and specific capacitance of 175 F g^{-1}). Ju et al. [192] studied electrospun ruthenium-PAN-based CN composite webs. The resultant membrane fiber diameter ranged from 100 to 350 nm, and the pore diameter of the film was 2.0 nm. The specific capacitance of the electrode with 7.31 wt% Ru reached 391 F g^{-1}, almost three times of that without Ru. However, Ru is a toxic rare-earth metal, so research has focused on other low cost metals such as nickel oxide-based materials [66,193,194]. Nataraj et al. [66] investigated the effect of nickel nitrate on the physical, thermal and morphological properties of carbon nanofibers. Results showed 5 wt% nickel nitrate increased the surface characteristics significantly. Li et al. [193] performed similar work and achieved a maximum capacitance of 164 F g^{-1} with 22.4 wt% nickel loading. Hosogai and Tsutsumi [194] made NiO/PVDF-HFP/acetylene black composite fibers. SEM pictures indicated partial melting of the fibers which likely contributed to the observed increase in specific capacitance.

Researchers also investigated the properties of PAN/MWCNT composite fibers that would impact their performance in supercapacitors [195–197]. Prilutsky et al. studied the effect of MWCNTs on the morphology of PAN fibers. Results indicate that embedded MWCNTs can promote the nucleation of carbon crystals during PAN carbonization [195]. Ju et al. [196] compared the electrochemical properties of activated carbon nanofibers, MWCNT/activated carbon nanofibers, and polypyrrole (PPy) coated MWCNT/activated carbon nanofibers. The addition of MWCNTs in activated carbon nanofibers led to higher surface area and higher electrical conductivity. The PPy coating on the surface of MWCNT/activated carbon nanofibers formed a good charge transfer complex, which resulted in a refined three-dimensional network. Guo et al. [197] did similar work by electrospinning and subsequently carbonizing and activating PAN/MWCNT composite fibers. The embedded MWCNTs improved the electrical conductivity and specific capacitance of the supercapacitor.

RuO_2 is an attractive material for use in supercapacitor electrodes, because it offers several oxidation states, high electrical conductivity, and electrochemical stability [198]. Depositing thin film RuO_2 on other materials is an effective way to lower cost. Ahn et al. demonstrated a RuO_2/TiO_2 composite manufactured by electrospinning [198]. Aqueous ruthenium chloride solution was electrodeposited onto electrospun TiO_2 substrate. Heat treated TiO_2 substrate enhanced the electrical conductivity and the composite electrode exhibited high capacitance and good cyclability. Besides carbon nanofibers, researchers also investigated other conductive materials as potential supercapacitor electrodes. A highly conductive $SrRuO_3$(SRO)-RuO_2 composite nanofiber mat was prepared through electrospinning and sintering [199]. The $SrRuO_3$(SRO)-RuO_2 electrode was sintered at 350 °C yielding a relatively high capacitance of 192 F g^{-1}.

3.5. Other materials

Besides these intensively studied fields, the electrospinning technique has also been utilized in other energy-related areas, for example, piezoelectric (including ferroelectric) and thermoelectric materials.

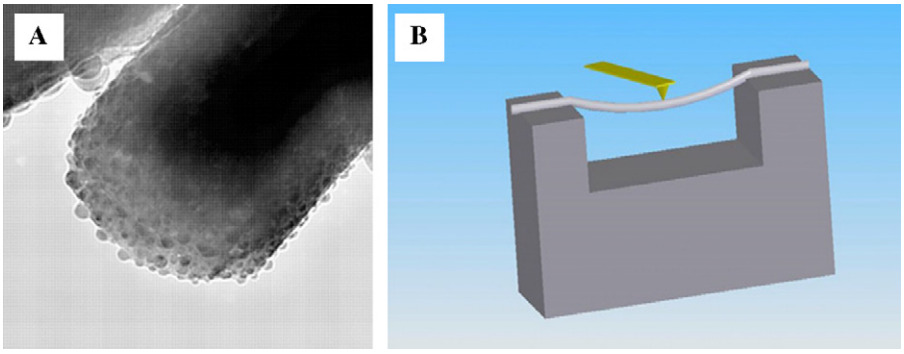

Fig. 19. (A) TEM images of PZT nanofiber, and (B) schematic illustration of a nanofiber pressed by the AFM tip (from Ref. [202]).

3.5.1. Piezoelectric materials

Piezoelectricity is the ability of some materials to convert electrical energy to mechanical and vice versa. Commonly used forms of piezoelectric materials are bulk and film. Electrospun piezoelectric nanofibers offer excellent flexibility and improved strength, so they are expected to be utilized in a wide variety of applications. Lead zirconate titanate ($PbZr_{1-x}$ Ti_xO_3, PZT) is a popular piezoelectric material with many advantages such as a high electromechanical coupling coefficient, high dielectric constant and high piezoelectric response [200]. Dharmaraj et al. fabricated PZT nanofibers by electrospinning [201]. The nanofibers had diameters ranging from 200 to 300 nm, and the formation of perovskite lead zirconate titanate was confirmed by XRD and FT–IR. Xu et al. [202] electrospun and studied the mechanical properties of an individual PZT nanofiber (Fig. 19), finding a lower elastic modulus of 42.99 GPa, possibly because of smaller grain size and fiber diameter. Hossain and Kim investigated the effect of acetic acid on the morphology of PZT electrospun nanofibers [203]. SEM and TEM results showed the PZT fibers processed with acetic acid were thinner and more compact. While PZT is commonly used because of its high piezoelectric response, lead is toxic to our environment, so great effort has been made pursuing synthetic lead-free piezoelectric alternatives. One such alternative, $Bi_{3.15}Nd_{0.85}Ti_3O_{12}$ (BNT) nanofibers with diameters ranging from 30 to 200 nm, have been fabricated by the sol–gel process and electrospinning. Tests showed that the BNT nanofibers had a higher effective piezoelectric coefficient and Curie temperature than that of bulk materials [204]. Vanadium-doped ZnO (V-ZnO) piezoelectric nanofibers were also prepared by electrospinning [205] and their nanoscale mechanical behavior was studied by nanoindentation [206]. The electrospun V-ZnO nanofibers had diameters ranging from 50 to 300 nm with good crystallinity. The V–ZnO nanofibers exhibited excellent piezoelectric properties comparable to bulk materials [205], but their modulus and hardness were lower than that of bulk materials [206].

3.5.2. Thermoelectric materials

Similar to piezoelectric materials, thermoelectric materials convert a potentially ambient source of energy to electricity. However, it harvests energy from temperature gradients rather than from mechanical strain. Electrospinning has played a role in developing new thermoelectric materials. Along them, sodium–cobalt oxide is a promising candidate due to its high chemical and thermal stability at high temperatures. Maensiri and Nuansing electrospun $NaCo_2O_4$ nanofibers [207] with diameters of about 20–200 nm, and XRD, Raman spectroscopy and SAED results suggested the formation of γ-$Na_xCo_2O_4$. $Ca_3Co_4O_9$ is another potential oxide material, and its layered structure benefits electronic transportation and phonon scattering. The figure of merit (ZT) value of a single crystalline $Ca_2Co_2O_5$ whisker was estimated to be 1.2 [208]. However, the ZT value was lower for polycrystalline $Ca_3Co_4O_9$ due to the random orientation and anisotropic nature of single grains [209,210]. Yin et al. [211] synthesized nanocrystalline thermoelectric $Ca_3Co_4O_9$ ceramics through a combination of electrospinning and spark plasma sintering. Results showed nanofiber-sintered $Ca_3Co_4O_9$ ceramics had much smaller grains and controllable grain orientation, resulting in improved thermoelectric properties.

4. Conclusions

Meeting global energy demands is one of the most pressing needs mankind faces in the 21st century. Nanofibers may play a key role in addressing these issues because of their unique structures and high surface area to volume ratios. Among the many nanofiber fabrication methods, electrospinning holds significant promise due to its comparative low cost and relatively high production rate. In addition, the required manufacturing hardware and operation parameters can be easily reconfigured to produce fibers with a variety of structures, such as core–shell, hollow or aligned fibers. Many kinds of materials have been synthesized through electrospinning, from conventional polymers to ceramics, metals, alloys, and composites fibers. The catalog of electrospun nanofiber products have potential applications addressing the material needs of advanced energy devices like fuel cells, solar cells and lithium-ion batteries. Current progress reveals that electrospinning technology will likely play an important role in the development of new clean energy technologies. However, there are technical and theoretical issues that must be addressed before 1D nanostructures can become common materials in commercial devices. First, it is difficult to achieve uniformity in the diameters of electrospun nanofibers below 50 nm. Second, there is still room to advance the theoretical modeling of the electrospinning process. Finally, current electrospinning processes commonly involve toxic and corrosive organic solvents in the preparation of precursor solutions. For future research, the fabrication of composite nanomaterials with particular functional groups may be a promising field. Addressing these concerns will require dedicated, interdisciplinary research around the world to ensure that electrospinning will reach its potential in fabricating nanosized materials for energy conversion applications.

Acknowledgments

This work was financially supported by NSF and AFOSR.

References

[1] OPEC Secretariat, World Oil Outlook 2009, Organization of Petroleum Exporting Countries, Vienna, 2009, pp. 21–76.
[2] E.I. Administration, International Energy Outlook 2009, U.S. Energy Information Administration, Washington, 2009, pp. 1–6.
[3] J.T. Kiehl, K.E. Trenberth, Bull. Am. Meteorol. Soc. 78 (1997) 197–208.
[4] C.R. Martin, Science 266 (1994) 1961–1966.
[5] B.B. Lakshmi, P.K. Dorhout, C.R. Martin, Chem. Mater. 9 (1997) 857–862.

[6] M. Steinhart, J.H. Wendorff, A. Greiner, R.B. Wehrspohn, K. Nielsch, J. Schilling, J. Choi, U. Gosele, Science 296 (2002) 1997.
[7] M. Law, J. Goldberger, P.D. Yang, Ann. Rev. Mater. Res. 34 (2004) 83–122.
[8] J.X. Huang, S. Virji, B.H. Weiller, R.B. Kaner, J. Am. Chem. Soc. 125 (2003) 314–315.
[9] X. Wang, Y.D. Li, J. Am. Chem. Soc. 124 (2002) 2880–2881.
[10] Y.G. Sun, Y.D. Yin, B.T. Mayers, T. Herricks, Y.N. Xia, Chem. Mater. 14 (2002) 4736–4745.
[11] A.A. Tseng, A. Notargiacomo, T.P. Chen, J. Vac. Sci. Technol. B 23 (2005) 877–894.
[12] D. Wouters, U.S. Schubert, Angew. Chem.-Int. Ed. 43 (2004) 2480–2495.
[13] J.D. Hartgerink, E. Beniash, S.I. Stupp, Science 294 (2001) 1684–1688.
[14] J.F. COOLEY, US Patent 692631, 1902.
[15] A. Formhals, US Patent 1975504, 1934.
[16] J. Doshi, D.H. Reneker, J. Electrostat. 35 (1995) 151–160.
[17] D.H. Reneker, I. Chun, Nanotechnology 7 (1996) 216–223.
[18] Z.M. Huang, Y.Z. Zhang, M. Kotaki, S. Ramakrishna, Compos. Sci. Technol. 63 (2003) 2223–2253.
[19] D. Li, Y.N. Xia, Adv. Mater. 16 (2004) 1151–1170.
[20] A. Greiner, J.H. Wendorff, Angew. Chem.-Int. Ed. 46 (2007) 5670–5703.
[21] G. Taylor, Proc. R. Soc. Lond. Ser. A, Math. Phys. Sci. 280 (1964) 383–397.
[22] A.L. Yarin, S. Koombhongse, D.H. Reneker, J. Appl. Phys. 89 (2001) 3018–3026.
[23] H. Fong, I. Chun, D.H. Reneker, Polymer 40 (1999) 4585–4592.
[24] L. Huang, R.A. McMillan, R.P. Apkarian, B. Pourdeyhimi, V.P. Conticello, E.L. Chaikof, Macromolecules 33 (2000) 2989–2997.
[25] H. Fong, W.D. Liu, C.S. Wang, R.A. Vaia, Polymer 43 (2002) 775–780.
[26] C.L. Casper, J.S. Stephens, N.G. Tassi, D.B. Chase, J.F. Rabolt, Macromolecules 37 (2004) 573–578.
[27] J.T. McCann, D. Li, Y.N. Xia, J. Mater. Chem. 15 (2005) 735–738.
[28] D. Li, Y.L. Wang, Y.N. Xia, Nano Lett. 3 (2003) 1167–1171.
[29] V. Thavasi, G. Singh, S. Ramakrishna, Energy Environ. Sci. 1 (2008) 205–221.
[30] W.J. Li, C.T. Laurencin, E.J. Caterson, R.S. Tuan, F.K. Ko, J. Biomed. Mater. Res. 60 (2002) 613–621.
[31] J.A. Matthews, G.E. Wnek, D.G. Simpson, G.L. Bowlin, Biomacromolecules 3 (2002) 232–238.
[32] H. Yoshimoto, Y.M. Shin, H. Terai, J.P. Vacanti, Biomaterials 24 (2003) 2077–2082.
[33] E.D. Boland, J.A. Matthews, K.J. Pawlowski, D.G. Simpson, G.E. Wnek, G.L. Bowlin, Front. Biosci. 9 (2004) 1422–1432.
[34] E.R. Kenawy, G.L. Bowlin, K. Mansfield, J. Layman, D.G. Simpson, E.H. Sanders, G.E. Wnek, J. Control. Rel. 81 (2002) 57–64.
[35] D.S. Katti, K.W. Robinson, F.K. Ko, C.T. Laurencin, J. Biomed. Mater. Res. Part B: Appl. Biomater. 70B (2004) 286–296.
[36] K. Kim, Y.K. Luu, C. Chang, D.F. Fang, B.S. Hsiao, B. Chu, M. Hadjiargyrou, J. Control. Rel. 98 (2004) 47–56.
[37] M.S. Khil, D.I. Cha, H.Y. Kim, I.S. Kim, N. Bhattarai, J. Biomed. Mater. Res. Part B: Appl. Biomater. 67B (2003) 675–679.
[38] K.S. Rho, L. Jeong, G. Lee, B.M. Seo, Y.J. Park, S.D. Hong, S. Roh, J.J. Cho, W.H. Park, B.M. Min, Biomaterials 27 (2006) 1452–1461.
[39] I.D. Kim, A. Rothschild, B.H. Lee, D.Y. Kim, S.M. Jo, H.L. Tuller, Nano Lett. 6 (2006) 2009–2013.
[40] J. Yoon, S.K. Chae, J.M. Kim, J. Am. Chem. Soc. 129 (2007) 3038–3039.
[41] Z.Y. Li, H.N. Zhang, W. Zheng, W. Wang, H.M. Huang, C. Wang, A.G. MacDiarmid, Y. Wei, J. Am. Chem. Soc. 130 (2008) 5036–5037.
[42] Z.W. Ma, M. Kotaki, S. Ramakrishna, J. Membr. Sci. 265 (2005) 115–123.
[43] R. Gopal, S. Kaur, Z.W. Ma, C. Chan, S. Ramakrishna, T. Matsuura, J. Membr. Sci. 281 (2006) 581–586.
[44] M. Bognitzk, H.Q. Hou, M. Ishaque, T. Frese, M. Hellwig, C. Schwarte, A. Schaper, J.H. Wendorff, A. Greiner, Adv. Mater. 12 (2000) 637–640.
[45] H. Schreuder-Gibson, P. Gibson, K. Senecal, M. Sennett, J. Walker, W. Yeomans, D. Ziegler, P.P. Tsai, J. Adv. Mater. 34 (2002) 44–55.
[46] M.M. Bergshoef, G.J. Vancso, Adv. Mater. 11 (1999) 1362–1365.
[47] J.S. Kim, D.H. Reneker, Polym. Compos. 20 (1999) 124–131.
[48] S. Ramakrishna, K. Fujihara, W.E. Teo, T. Yong, Z.W. Ma, R. Ramaseshan, Mater. Today 9 (2006) 40–50.
[49] Y.S. Kim, S.H. Nam, H.S. Shim, H.J. Ahn, M. Anand, W.B. Kim, Electrochem. Commun. 10 (2008) 1016–1019.
[50] H.J. Kim, Y.S. Kim, M.H. Seo, S.M. Choi, W.B. Kim, Electrochem. Commun. 11 (2009) 446–449.
[51] J.L. Shui, J.C.M. Li, Nano Lett. 9 (2009) 1307–1314.
[52] H.J. Kim, Y.S. Kim, M.H. Seo, S.M. Choi, J. Cho, G.W. Huber, W.B. Kim, Electrochem. Commun. 12 (2010) 32–35.
[53] U.A. Paulus, T.J. Schmidt, H.A. Gasteiger, R.J. Behm, J. Electroanal. Chem. 495 (2001) 134–145.
[54] Z.L. Liu, X.H. Lin, J.Y. Lee, W. Zhang, M. Han, L.M. Gan, Langmuir 18 (2002) 4054–4060.
[55] W.Z. Li, C.H. Liang, W.J. Zhou, J.S. Qiu, Z.H. Zhou, G.Q. Sun, Q. Xin, J. Phys. Chem. B 107 (2003) 6292–6299.
[56] C. Wang, M. Waje, X. Wang, J.M. Tang, R.C. Haddon, Y.S. Yan, Nano Lett. 4 (2004) 345–348.
[57] C.A. Bessel, K. Laubernds, N.M. Rodriguez, R.T.K. Baker, J. Phys. Chem. B 105 (2001) 1115–1118.
[58] E. Auer, A. Freund, J. Pietsch, T. Tacke, Appl. Catal. A: Gen. 173 (1998) 259–271.
[59] H.E. Vandam, H. Vanbekkum, J. Catal. 131 (1991) 335–349.
[60] F. Rodriguez-Reinoso, Carbon 36 (1998) 159–175.
[61] F.J. Liu, L.M. Huang, T.C. Wen, A. Gopalan, Synth. Met. 157 (2007) 651–658.
[62] E. Formo, Z.M. Peng, E. Lee, X.M. Lu, H. Yang, Y.N. Xia, J. Phys. Chem. C 112 (2008) 9970–9975.
[63] E.S. Steigerwalt, G.A. Deluga, C.M. Lukehart, J. Phys. Chem. B 106 (2002) 760–766.
[64] E.S. Steigerwalt, G.A. Deluga, C.M. Lukehart, J. Nanosci. Nanotechnol. 3 (2003) 247–251.
[65] J.H. Park, Y.W. Ju, S.H. Park, H.R. Jung, K.S. Yang, W.J. Lee, J. Appl. Electrochem. 39 (2009) 1229–1236.
[66] S.K. Nataraj, B.H. Kim, J.H. Yun, D.H. Lee, T.M. Aminabhavi, K.S. Yang, Mater. Sci. Eng. B: Adv. Funct. Solid-State Mater. 162 (2009) 75–81.
[67] N.T. Xuyen, H.K. Jeong, G. Kim, K.P. So, K.H. An, Y.H. Lee, J. Mater. Chem. 19 (2009) 1283–1288.
[68] M.Y. Li, S.Z. Zhao, G.Y. Han, B.S. Yang, J. Power Sources 191 (2009) 351–356.
[69] Z. Lin, L.W. Ji, M.D. Woodroof, Y.F. Yao, W. Krause, X.W. Zhang, J. Phys. Chem. C 114 (2010) 3791–3797.
[70] X.M. Liu, M.Y. Li, G.Y. Han, J.H. Dong, Electrochim. Acta 55 (2010) 2983–2990.
[71] J.S. Huang, H.Q. Hou, T.Y. You, Electrochem. Commun. 11 (2009) 1281–1284.
[72] L. Su, W.Z. Jia, A. Schempf, Y. Ding, Y. Lei, J. Phys. Chem. C 113 (2009) 16174–16180.
[73] S.H. Hong, S.A. Lee, J.D. Nam, Y.K. Lee, T.S. Kim, S. Won, Macromol. Res. 16 (2008) 204–211.
[74] H. Chen, J.D. Snyder, Y.A. Elabd, Macromolecules 41 (2008) 128–135.
[75] R. Bajon, S. Balaji, S.M. Guo, J. Fuel Cell Sci. Technol. 6 (2009) 031004.
[76] S.W. Choi, Y.Z. Fu, Y.R. Ahn, S.M. Jo, A. Manthiram, J. Power Sources 180 (2008) 167–171.
[77] Y.B. Chen, J. Guo, H. Kim, React. Funct. Polym. 70 (2010) 69–74.
[78] T. Tamura, H. Kawakami, Nano Lett. 10 (2010) 1324–1328.
[79] B. Oregan, M. Gratzel, Nature 353 (1991) 737–740.
[80] M.Y. Song, Y.R. Ahn, S.M. Jo, D.Y. Kim, J.P. Ahn, Appl. Phys. Lett. 87 (2005) 113113.
[81] K. Mukherjee, T.H. Teng, R. Jose, S. Ramakrishna, Appl. Phys. Lett. 95 (2009) 012101.
[82] A.R.S. Priya, A. Subramania, Y.S. Jung, K.J. Kim, Langmuir 24 (2008) 9816–9819.
[83] Y.X. Li, J. Hagen, W. Schaffrath, P. Otschik, D. Haarer, Sol. Energy Mater. Sol. Cells 56 (1999) 167–174.
[84] K. Srikanth, M.M. Rahman, H. Tanaka, K.M. Krishna, T. Soga, M.K. Mishra, T. Jimbo, M. Umeno, Sol. Energy Mater. Sol. Cells 65 (2001) 171–177.
[85] E. Lancelle-Beltran, P. Prene, C. Boscher, P. Belleville, P. Buvat, S. Lambert, F. Guillet, C. Boissiere, D. Grosso, C. Sanchez, Chem. Mat. 18 (2006) 6152–6156.
[86] T.L. Ma, T. Kida, M. Akiyama, K. Inoue, S.J. Tsunematsu, K. Yao, H. Noma, E. Abe, Electrochem. Commun. 5 (2003) 369–372.
[87] M. Adachi, Y. Murata, J. Takao, J.T. Jiu, M. Sakamoto, F.M. Wang, J. Am. Chem. Soc. 126 (2004) 14943–14949.
[88] S. Chuangchote, T. Sagawa, S. Yoshikawa, Appl. Phys. Lett. 93 (2008) 033310.
[89] W. Kubo, T. Kitamura, K. Hanabusa, Y. Wada, S. Yanagida, Chem. Commun. (2002) 374–375.
[90] Q.B. Meng, K. Takahashi, X.T. Zhang, I. Sutanto, T.N. Rao, O. Sato, A. Fujishima, H. Watanabe, T. Nakamori, M. Uragami, Langmuir 19 (2003) 3572–3574.
[91] P. Wang, S.M. Zakeeruddin, P. Comte, I. Exnar, M. Gratzel, J. Am. Chem. Soc. 125 (2003) 1166–1167.
[92] A.F. Nogueira, J.R. Durrant, M.A. De Paoli, Adv. Mater. 13 (2001) 826–830.
[93] P. Wang, S.M. Zakeeruddin, J.E. Moser, M.K. Nazeeruddin, T. Sekiguchi, M. Gratzel, Nat. Mater. 2 (2003) 402–407.
[94] R. Chandrasekar, L.F. Zhang, J.Y. Howe, N.E. Hedin, Y. Zhang, H. Fong, J. Mater. Sci. 44 (2009) 1198–1205.
[95] M.Y. Song, D.K. Kim, S.M. Jo, D.Y. Kim, Synth. Met. 155 (2005) 635–638.
[96] M.Y. Song, D.K. Kim, K.J. Ihn, S.M. Jo, D.Y. Kim, Synth. Met. 153 (2005) 77–80.
[97] S.M. Jo, M.Y. Song, Y.R. Ahn, C.R. Park, D.Y. Kim, J. Macromol. Sci.-Pure Appl. Chem. A42 (2005) 1529–1540.
[98] M.Y. Song, D.K. Kim, K.J. Ihn, S.M. Jo, D.Y. Kim, Nanotechnology 15 (2004) 1861–1865.
[99] H.S. Shim, J.W. Kim, W.B. Kim, J. Nanosci. Nanotechnol. 9 (2009) 4721–4726.
[100] K. Fujihara, A. Kumar, R. Jose, S. Ramakrishna, S. Uchida, Nanotechnology 18 (2007) 365709.
[101] B. Tan, Y.Y. Wu, J. Phys. Chem. B 110 (2006) 15932–15938.
[102] K. Onozuka, B. Ding, Y. Tsuge, T. Naka, M. Yamazaki, S. Sugi, S. Ohno, M. Yoshikawa, S. Shiratori, Nanotechnology 17 (2006) 1026–1031.
[103] R. Zhu, C.Y. Jiang, X.Z. Liu, B. Liu, A. Kumar, S. Ramakrishna, Appl. Phys. Lett. 93 (2008) 013102.
[104] B.H. Lee, M.Y. Song, S.Y. Jang, S.M. Jo, S.Y. Kwak, D.Y. Kim, J. Phys. Chem. C 113 (2009) 21453–21457.
[105] S.H. Kang, S.H. Choi, M.S. Kang, J.Y. Kim, H.S. Kim, T. Hyeon, Y.E. Sung, Adv. Mater. 20 (2008) 54–58.
[106] G.J. Hu, X.F. Meng, X.Y. Feng, Y.F. Ding, S.M. Zhang, M.S. Yang, J. Mater. Sci. 42 (2007) 7162–7170.
[107] C. Bauer, G. Boschloo, E. Mukhtar, A. Hagfeldt, J. Phys. Chem. B 105 (2001) 5585–5588.
[108] I.D. Kim, J.M. Hong, B.H. Lee, D.Y. Kim, E.K. Jeon, D.K. Choi, D.J. Yang, Appl. Phys. Lett. 91 (2007) 163109.
[109] W. Zhang, R. Zhu, X.Z. Liu, B. Liu, S. Ramakrishna, Appl. Phys. Lett. 95 (2009) 043304.
[110] J.B. Baxter, E.S. Aydil, Appl. Phys. Lett. 86 (2005) 053114.
[111] A.B.F. Martinson, J.W. Elam, J.T. Hupp, M.J. Pellin, Nano Lett. 7 (2007) 2183–2187.
[112] M. Saito, S. Fujihara, Energy Environ. Sci. 1 (2008) 280–283.
[113] J.J. Wu, G.R. Chen, H.H. Yang, C.H. Ku, J.Y. Lai, Appl. Phys. Lett. 90 (2007) 213109.

[114] L.N. Liu, B. Li, J. Zhang, R.F. Qin, H.F. Zhao, X.G. Ren, Mater. Res. Bull. 44 (2009) 2081–2086.
[115] F. Iskandar, A.B. Suryamas, M. Kawabe, M.M. Munir, K. Okuyama, T. Tarao, T. Nishitani, Jpn. J. Appl. Phys. 49 (2010) 010213.
[116] S.H. Park, J.U. Kim, S.Y. Lee, W.K. Lee, J.K. Lee, M.R. Kim, J. Nanosci. Nanotechnol. 8 (2008) 4889–4894.
[117] J.U. Kim, S.H. Park, H.J. Choi, W.K. Lee, J.K. Lee, M.R. Kim, Sol. Energy Mater. Sol. Cells 93 (2009) 803–807.
[118] N.J. Dudney, Mater. Sci. Eng. B: Solid State Mater. Adv. Technol. 116 (2005) 245–249.
[119] M.M. Thackeray, W.I.F. David, P.G. Bruce, J.B. Goodenough, Mater. Res. Bull. 18 (1983) 461–472.
[120] H.F. Gibbard, J. Power Sources 26 (1989) 81–91.
[121] E. Plichta, S. Slane, M. Uchiyama, M. Salomon, D. Chua, W.B. Ebner, H.W. Lin, J. Electrochem. Soc. 136 (1989) 1865–1869.
[122] N.C. Li, C.J. Patrissi, G.L. Che, C.R. Martin, J. Electrochem. Soc. 147 (2000) 2044–2049.
[123] P.R. Bueno, E.R. Leite, J. Phys. Chem. B 107 (2003) 8868–8877.
[124] Y.X. Gu, D.R. Chen, M.L. Jiao, J. Phys. Chem. B 109 (2005) 17901–17906.
[125] C.L. Shao, N. Yu, Y.C. Liu, R.X. Mu, J. Phys. Chem. Solids 67 (2006) 1423–1426.
[126] H.W. Lu, L. Yu, W. Zeng, Y.S. Li, Z.W. Fu, Electrochem. Solid State Lett. 11 (2008) A140–A144.
[127] Z.X. Wang, C.A. Wu, L.J. Liu, F. Wu, L.Q. Chen, X.J. Huang, J. Electrochem. Soc. 149 (2002) A466–A471.
[128] Z.X. Wang, X.J. Huang, L.Q. Chen, J. Electrochem. Soc. 151 (2004) A1641–A1652.
[129] Y.X. Gu, D.R. Chen, X.L. Jiao, F.F. Liu, J. Mater. Chem. 17 (2007) 1769–1776.
[130] Y.H. Ding, P. Zhang, Y. Jiang, D.S. Gao, Solid State Ionics 178 (2007) 967–971.
[131] Y.S. He, Z.F. Ma, X.Z. Liao, Y. Jiang, J. Power Sources 163 (2007) 1053–1058.
[132] Y.H. Ding, P. Zhang, Z.L. Long, Y. Jiang, F. Xu, J. Alloys Compd. 487 (2009) 507–510.
[133] K. Sun, H.W. Lu, D. Li, W. Zeng, Y.S. Li, Z.W. Fu, J. Inorg. Mater. 24 (2009) 357–360.
[134] S.L. Bewlay, K. Konstantinov, G.X. Wang, S.X. Dou, H.K. Liu, Mater. Lett. 58 (2004) 1788–1791.
[135] E. Hosono, Y.G. Wang, N. Kida, M. Enomoto, N. Kojima, M. Okubo, H. Matsuda, Y. Saito, T. Kudo, I. Honma, H.S. Zhou, ACS Appl. Mater. Interfaces 2 (2010) 212–218.
[136] M. Yoshio, H.Y. Wang, K. Fukuda, Y. Hara, Y. Adachi, J. Electrochem. Soc. 147 (2000) 1245–1250.
[137] M.N. Obrovac, L. Christensen, Electrochem. Solid State Lett. 7 (2004) A93–A96.
[138] L.W. Ji, X.W. Zhang, Electrochem. Commun. 11 (2009) 1146–1149.
[139] L.W. Ji, K.H. Jung, A.J. Medford, X.W. Zhang, J. Mater. Chem. 19 (2009) 4992–4997.
[140] X. Fan, L. Zou, Y.P. Zheng, F.Y. Kang, W.C. Shen, Electrochem. Solid State Lett. 12 (2009) A199–A201.
[141] J.M. Tarascon, M. Armand, Nature 414 (2001) 359–367.
[142] L. Wang, Y. Yu, P.C. Chen, D.W. Zhang, C.H. Chen, J. Power Sources 183 (2008) 717–723.
[143] L.W. Ji, X.W. Zhang, Electrochem. Commun. 11 (2009) 795–798.
[144] L.W. Ji, A.J. Medford, X.W. Zhang, J. Mater. Chem. 19 (2009) 5593–5601.
[145] J.G. Ren, X.M. He, L. Wang, W.H. Pu, C.Y. Jiang, C.R. Wan, Electrochim. Acta 52 (2007) 2447–2452.
[146] L.W. Ji, Z. Lin, A.J. Medford, X.W. Zhang, Chem.-A Eur. J. 15 (2009) 10718–10722.
[147] L.W. Ji, Z. Lin, R. Zhou, Q. Shi, O. Toprakci, A.J. Medford, C.R. Millns, X.W. Zhang, Electrochim. Acta 55 (2010) 1605–1611.
[148] Y. Yu, L. Gu, C.B. Zhu, P.A. van Aken, J. Maier, J. Am. Chem. Soc. 131 (2009) 15984–15985.
[149] Y. Yu, L. Gu, C.L. Wang, A. Dhanabalan, P.A. van Aken, J. Maier, Angew. Chem.-Int. Ed. 48 (2009) 6485–6489.
[150] L. Zou, L. Gan, F.Y. Kang, M.X. Wang, W.C. Shen, Z.H. Huang, J. Power Sources 195 (2010) 1216–1220.
[151] L. Wang, Y. Yu, P.C. Chen, C.H. Chen, Scripta Mater. 58 (2008) 405–408.
[152] P. Poizot, S. Laruelle, S. Grugeon, L. Dupont, J.M. Tarascon, Nature 407 (2000) 496–499.
[153] Y. Wang, Q.Z. Qin, J. Electrochem. Soc. 149 (2002) A873–A878.
[154] L. Yuan, Z.P. Guo, K. Konstantinov, P. Munroe, H.K. Liu, Electrochem. Solid State Lett. 9 (2006) A524–A528.
[155] H.W. Lu, D. Li, K. Sun, Y.S. Li, Z.W. Fu, Solid State Sciences 11 (2009) 982–987.
[156] Q. Fan, M.S. Whittingham, Electrochem. Solid State Lett. 10 (2007) A48–A51.
[157] L.W. Ji, X.W. Zhang, Nanotechnology 20 (2009) 155705.
[158] L.W. Ji, X.W. Zhang, Electrochem. Commun. 11 (2009) 684–687.
[159] L.W. Ji, Z. Lin, A.J. Medford, X.W. Zhang, Carbon 47 (2009) 3346–3354.
[160] M. Wagemaker, A.P.M. Kentgens, F.M. Mulder, Nature 418 (2002) 397–399.
[161] H. Qiao, Y.W. Wang, L.F. Xiao, L.Z. Zhang, Electrochem. Commun. 10 (2008) 1280–1283.
[162] M.V. Reddy, R. Jose, T.H. Teng, B.V.R. Chowdari, S. Ramakrishna, Electrochim. Acta 55 (2010) 3109–3117.
[163] W.Y. Li, L.N. Xu, J. Chen, Adv. Funct. Mater. 15 (2005) 851–857.
[164] Y.X. Gu, F.F. Jian, X. Wang, Thin Solid Films 517 (2008) 652–655.
[165] Y.H. Ding, P. Zhang, Z.L. Long, Y. Jiang, J.N. Huang, W.J. Yan, G. Liu, Mater. Lett. 62 (2008) 3410–3412.
[166] S. Abbrent, J. Plestil, D. Hlavata, J. Lindgren, J. Tegenfeldt, A. Wendsjo, Polymer 42 (2001) 1407–1416.
[167] S.W. Choi, S.M. Jo, W.S. Lee, Y.R. Kim, Adv. Mater. 15 (2003) 2027–2032.
[168] K. Gao, X.G. Hu, C.S. Dai, T.F. Yi, Mater. Sci. Eng. B: Solid State Mater. Adv. Technol. 131 (2006) 100–105.
[169] M.A. Kader, S.K. Kwak, S.L. Kang, J.H. Ahn, C. Nah, Polym. Int. 57 (2008) 1199–1205.
[170] J.R. Kim, S.W. Choi, S.M. Jo, W.S. Lee, B.C. Kim, J. Electrochem. Soc. 152 (2005) A295–A300.
[171] J.K. Kim, J. Manuel, G.S. Chauhan, J.H. Ahn, H.S. Ryu, Electrochim. Acta 55 (2010) 1366–1372.
[172] Y.H. Ding, P. Zhang, Z.L. Long, Y. Jiang, F. Xu, W. Di, J. Membr. Sci. 329 (2009) 56–59.
[173] A.I. Gopalan, P. Santhosh, K.M. Manesh, J.H. Nho, S.H. Kim, C.G. Hwang, K.P. Lee, J. Membr. Sci. 325 (2008) 683–690.
[174] K.U. Jeong, H.D. Chae, C. Il Lim, H.K. Lee, J.H. Ahn, C. Nah, Polym. Int. 59 (2010) 249–255.
[175] F. Croce, G.B. Appetecchi, L. Persi, B. Scrosati, Nature 394 (1998) 456–458.
[176] F. Croce, R. Curini, A. Martinelli, L. Persi, F. Ronci, B. Scrosati, R. Caminiti, J. Phys. Chem. B 103 (1999) 10632–10638.
[177] J.K. Kim, G. Cheruvally, X. Li, J.H. Ahn, K.W. Kim, H.J. Ahn, J. Power Sources 178 (2008) 815–820.
[178] P. Raghaven, J.W. Choi, J.H. Ahn, G. Cheruvally, G.S. Chauhan, H.J. Ahn, C. Nah, J. Power Sources 184 (2008) 437–443.
[179] Q.Z. Xiao, Z.H. Li, D.S. Gao, H.L. Zhang, J. Membr. Sci. 326 (2009) 260–264.
[180] T.H. Cho, T. Sakai, S. Tanase, K. Kimura, Y. Kondo, T. Tarao, M. Tanaka, Electrochem. Solid State Lett. 10 (2007) A159–A162.
[181] T.H. Cho, M. Tanaka, H. Onishi, Y. Kondo, T. Nakamura, H. Yamazaki, S. Tanase, T. Sakai, J. Power Sources 181 (2008) 155–160.
[182] Y.W. Ju, J.H. Park, H.R. Jung, W.J. Lee, Electrochim. Acta 52 (2007) 4841–4847.
[183] J. Gamby, P.L. Taberna, P. Simon, J.F. Fauvarque, M. Chesneau, J. Power Sources 101 (2001) 109–116.
[184] J. Chmiola, G. Yushin, Y. Gogotsi, C. Portet, P. Simon, P.L. Taberna, Science 313 (2006) 1760–1763.
[185] J. Lee, J. Kim, T. Hyeon, Adv. Mater. 18 (2006) 2073–2094.
[186] A.G. Pandolfo, A.F. Hollenkamp, J. Power Sources 157 (2006) 11–27.
[187] C. Kim, S.H. Park, W.J. Lee, K.S. Yang, Electrochim. Acta 50 (2004) 877–881.
[188] C. Kim, J. Power Sources 142 (2005) 382–388.
[189] C. Kim, B.T.N. Ngoc, K.S. Yang, M. Kojima, Y.A. Kim, Y.J. Kim, M. Endo, S.C. Yang, Adv. Mater. 19 (2007) 2341–2346.
[190] C. Kim, K.S. Yang, W.J. Lee, Electrochem. Solid State Lett. 7 (2004) A397–A399.
[191] C. Kim, Y.O. Choi, W.J. Lee, K.S. Yang, Electrochim. Acta 50 (2004) 883–887.
[192] Y.W. Ju, G.R. Choi, H.R. Jung, C. Kim, K.S. Yang, W.J. Lee, J. Electrochem. Soc. 154 (2007) A192–A197.
[193] J. Li, E.H. Liu, W. Li, X.Y. Meng, S.T. Tan, J. Alloys Compd. 478 (2009) 371–374.
[194] S. Hosogai, H. Tsutsumi, J. Power Sources 194 (2009) 1213–1217.
[195] S. Prilutsky, E. Zussman, Y. Cohen, Nanotechnology 19 (2008) 165603.
[196] Y.W. Ju, G.R. Choi, H.R. Jung, W.J. Lee, Electrochim. Acta 53 (2008) 5796–5803.
[197] Q.H. Guo, X.P. Zhou, X.Y. Li, S.L. Chen, A. Seema, A. Greiner, H.Q. Hou, J. Mater. Chem. 19 (2009) 2810–2816.
[198] Y.R. Ahn, C.R. Park, S.M. Jo, D.Y. Kim, Appl. Phys. Lett. 90 (2007) 122106.
[199] T.S. Hyun, H.G. Kim, I.D. Kim, J. Power Sources 195 (2010) 1522–1528.
[200] R. Guo, L.E. Cross, S.E. Park, B. Noheda, D.E. Cox, G. Shirane, Phys. Rev. Lett. 84 (2000) 5423–5426.
[201] N. Dharmaraj, C.H. Kim, H.Y. Kim, Mater. Lett. 59 (2005) 3085–3089.
[202] S.Y. Xu, Y. Shi, S.G. Kim, Nanotechnology 17 (2006) 4497–4501.
[203] M. Hossain, A. Kim, Mater. Lett. 63 (2009) 789–792.
[204] M. Liao, X.L. Zhong, J.B. Wang, S.H. Xie, Y.C. Zhou, Appl. Phys. Lett. 96 (2010) 012904.
[205] Y.Q. Chen, X.J. Zheng, X. Feng, Nanotechnology 21 (2010) 055708.
[206] Y.Q. Chen, X.J. Zheng, S.X. Mao, W. Li, J. Appl. Phys. 107 (2010) 094302.
[207] S. Maensiri, W. Nuansing, Mater. Chem. Phys. 99 (2006) 104–108.
[208] R. Funahashi, I. Matsubara, H. Ikuta, T. Takeuchi, U. Mizutani, S. Sodeoka, Jpn. J. Appl. Phys. Part 2: Lett. 39 (2000) L1127–L1129.
[209] E. Guilmeau, R. Funahashi, M. Mikami, K. Chong, D. Chateigner, Appl. Phys. Lett. 85 (2004) 1490–1492.
[210] S. Bhattacharya, D.K. Aswal, A. Singh, C. Thinaharan, N. Kulkarni, S.K. Gupta, J.V. Yakhmi, J. Cryst. Growth 277 (2005) 246–251.
[211] T.F. Yin, D.W. Liu, Y. Ou, F.Y. Ma, S.H. Xie, J.F. Li, J.Y. Li, J. Phys. Chem. C 114 (2010) 10061–10065.